A FINITE ELEMENT MODEL TO STUDY THE MICROSCOPIC BEHAVIOR OF PLAIN CONCRETE

by

ATAULLAH MAHER

DAVID DARWIN

A Report on a Research Project Sponsored by

The National Science Foundation

Research Grant ENG76-09444

CRINC REPORT - SL-76-02

November 1976

THE UNIVERSITY OF KANSAS CENTER FOR RESEARCH, INC.

2291 Irving Hill Rd.—Campus West Lawrence, Kansas 66044

A FINITE ELEMENT MODEL TO STUDY THE MICROSCOPIC BEHAVIOR OF PLAIN CONCRETE

by

ATAULLAH MAHER

DAVID DARWIN

A Report on a Research Project Sponsored by

THE NATIONAL SCIENCE FOUNDATION

Research Grant ENG76-09444

UNIVERSITY OF KANSAS

LAWRENCE, KANSAS

November 1976

ACKNOWLEDGEMENTS

This report is based on a thesis submitted by Ataullah Maher in partial fulfillment of the requirements for the Master's degree. The support of Mr. Maher's graduate study by University of Kansas General Research Allocations No. 3840-5038 and 3120-5038 is gratefully acknowledged.

The numerical calculations were performed on the Honeywell 635 and 66/60 systems of the Computer Center of the University of Kansas.

This study was funded in part under National Science Foundation Research Grant No. ENG76-09444.

TABLE OF CONTENTS

Chapter		Page
1	INTRODUCTION	1
	1.1 General	1
	1.2 Previous Work	2
	1.3 Object and Scope	5
2	MATERIAL MODEL	6
	2.1 General	6
	2.2 Mortar	6
	2.3 Aggregate	14
	2.4 Mortar-Aggregate Interface	15
3	FINITE ELEMENT ANALYSIS	19
	3.1 Isoparametric Element	19
	3.2 Analysis Procedure	19
	3.3 Convergence Criteria	25
4	NUMERICAL STUDY	27
	4.1 General	27
	4.2 Plan of Study	27
	4.3 Results and Discussion	29
5	SUMMARY AND CONCLUSIONS	38
	5.1 Summary	38
	5.2 Conclusions	38
	5.3 Recommendations for Future Study	39
REFERENCES		41
APPENDIX		
A	CONSTITUTIVE RELATIONS FOR AN ORTHOTROPIC MATERIAL	44
B	PROPERTIES OF THE FINITE ELEMENT	48

LIST OF TABLES

Table		Page
4.1	Stresses and Strains in Concrete at Different Stages of Cracking for Normal Strength of Interface	54
4.2	Stresses and Strains in Concrete at Different Stages of Cracking for Zero Tensile and Cohesive Strength of Interface	55
4.3	Stresses and Strains in Concrete at Different Stages of Cracking for Zero Cohesive and Tensile Strengths and Zero Angle of Internal Friction of Interface	56

LIST OF FIGURES

Figure		Page
2.1	Equivalent Uniaxial Stress-Strain Curve	57
2.2	Experimental and Analytical Strength Envelopes for Mortar	58
2.3	Comparison of Experimental and Analytical Uniaxial Loading Curves for Mortar	59
2.4	Comparison of Analytical and Experimental Biaxial Loading Curves for Mortar, $\alpha = 0.2$	60
2.5	Comparison of Experimental and Analytical Biaxial Loading Curves for Mortar, $\alpha = 0.5$	61
2.6	Comparison of Experimental and Analytical Biaxial Loading Curves for Mortar, $\alpha = 1.0$	62
2.7	Stress-Strain Curves for Stone	63
2.8	Strength Envelope for Interface	64
3.1.a	Correction of Loads	65
3.1.b	Correction of Stresses	65
4.1	Shah and Winter's "Structural Unit" of Concrete	66
4.2	Finite Element Model	67
4.3	Uniaxial Stress-Strain Curves for Concrete with Normal Strength of Interface	68
4.4	Cracking Maps for Concrete with Normal Strengths of Interface	69
4.5	Stress-Strain Curve for Concrete with Infinite Interfacial Strength	70

Figure		Page
4.6	Stress-Strain Curve for Concrete with Zero Tensile and Cohesive Strength of Interface	71
4.7	Cracking Maps for Concrete with Zero Tensile and Cohesive Interfacial Strength	72
4.8	Stress-Strain Curves for Concrete with Zero Interfacial Strength	73
4.9	Cracking Maps for Concrete with Zero Interfacial Strength	74
4.10	Analytical Stress-Strain Curves for Concrete with Normal Interfacial Strength and Nonlinear Mortar	75
4.11	Comparison of Experimental and Analytical Stress-Strain Curves	76
4.12	Buyukozturk's Model of Concrete	77
4.13	Stress-Strain Curves for Concrete with Linear Representation of Mortar	78
4.14	Stress-Strain Curves for Concrete with Nonlinear Mortar	79
4.15	Analytical Biaxial Stress-Strain Curves	80
4.16	Comparison of Experimental and Analytical Biaxial Stress-Strain Curves for Concrete	81
4.17	Biaxial Strength Envelopes	82

CHAPTER 1

INTRODUCTION

1.1 GENERAL Concrete is an important construction material. Inexpensive, strong and easily adaptable, it is widely used throughout the world. Until not long ago, it was idealized as a linear elastic, brittle material. However, concrete is a nonlinear material. During the last fifteen years it has been established that the load-deflection behavior of concrete is closely related to its microscopic behavior. Investigations (10, 12, 13, 14) have directly or indirectly related the shape of the stress-strain curve to the irreversible formation of microcracks, microscopic cracks between mortar and aggregate and within mortar. The relative significance of these cracks has yet to be determined. Under biaxial load conditions, the behavior of concrete is different from that under uniaxial loading (17, 20, 23). The role played by restrained cracking and nonlinearity of mortar has not been established.

The fact that concrete is a major construction material, requires that its load deflection behavior be clearly understood. A better understanding of the microscopic and macroscopic behavior of concrete will make more economical use of this material possible. This better understanding requires continued study. A tool in the study is the analytical model, which may be used to help determine the importance of microscopic behavior and its effect on the macroscopic behavior of concrete. The finite element method is an effective analytical technique. This report presents a finite element model for investigating the uniaxial and biaxial behavior of concrete.

1.2. PREVIOUS WORK As early as 1927, Brandtzaeg pointed out that the failure of concrete is related to progressive internal splitting (10). Hsu, Slate, Sturman and Winter (12) investigated the case of plain concrete in uniaxial compression. They found that the bond between aggregate and mortar is the weakest link in the heterogeneous concrete system and that microcracks exist at the interface between aggregate and mortar before concrete is subjected to any load. The stress-strain curve begins to deviate from a straight line at about 30% of the ultimate load, when these bond cracks begin to increase in length, width and number. At about 70-90% of the ultimate load, cracks through the mortar (mortar cracks) begin to increase rapidly, bridging between bond cracks and resulting in continuous crack patterns. Tests (16, 22, 31) have demonstrated that this load corresponds to the long term strength of concrete. Hsu and Slate (14) investigated the tensile bond strength of the mortar-aggregate interface and Hsu (13) showed analytically that tensile stresses develop at the interface when mortar shrinks during hydration. Slate and Matheus (32) found that volume changes of the order necessary to cause these microcracks do occur in portland cement concrete. Ash (1) demonstrated that some of these microcracks which exist in concrete specimens before loading, are formed during casting of the concrete due to bleeding. Taylor and Broms (33) studied the compression-shear bond strength of unconfined slabs of rock in mortar, and determined that the failure of the interface could be described by the Mohr-Coulomb Theory. Shah and Winter (28) studied confined rock slabs restrained from sliding by the surrounding mortar matrix, at various inclinations with respect to the

load. They found that when the unconfined strength of the interface is lost, sliding is resisted by the friction between aggregate and mortar and the confining mortar. Using their findings they developed an analytical model of concrete.

Conflicting results have been obtained in studies of the effect of mortar-aggregate bond strength on the behavior of portland cement concrete. A large effect on the strength of concrete has been indicated by two studies (4, 30), while a third study (6) indicates a relatively small effect.

Studies of the biaxial behavior of concrete (17, 20) indicate different strengths under different combinations of load. Under biaxial compression an increase, and under combined tension and compression a decrease in strength is observed. Essentially no change is observed in biaxial tensile strength. Analytical failure envelopes (7, 18, 21) have been proposed based on these experimental results. Liu's experimental work (19) showed that mortar is a nonlinear material and that its behavior under biaxial loading is different from its uniaxial behavior.

Several attempts have been made to explain the complex behavior of concrete with the help of models. A brief, critical review of various models is presented by Buyukozturk (2). Hurley (15) employed Shah and Winter's model (28) of concrete to investigate the behavior of plain concrete under uniaxial loading using the finite element method. Buyukozturk introduced experimental and analytical models of concrete based on the Shah and Winter model. Using the Mohr-Coulomb Theory for sliding failure of interface and the Maximum Stress Theory

for failure of mortar, he obtained a good match of cracking patterns between the analytical and experimental models. However, his analytical model which employed linear elastic representations of aggregate and mortar was considerably stiffer than the experimental model. Carino and Slate (3) found that an adaptation of the Maximum Strain Theory worked well for Buyukozturk's physical model of concrete, under tension-compression and tension-tension loadings.

Studies have been made to investigate the applicability of Griffith's criteria of fracture to the failure of concrete. A thorough review of work on this area has been presented by Radjy and Hansen (25). Some other failure criteria have also been suggested (34, 35). Niva and Kobayashi (24) proposed a failure criterion for cement mortar under biaxial compression, based on Griffith's criteria of fracture.

Various workers have attempted to model the nonlinear load-deflection behavior of concrete. Early investigations suggested simple parabolic representations of the load deflection curve (9, 27) for uniaxial loading of concrete. Kupfer and Gerstle (18) presented an analytical model of concrete, as an isotropic material under monotonic biaxial loading. Liu et al (20,21) modeled concrete as a nonlinear orthotropic material. Darwin and Pecknold (7, 8) developed a numerical representation for the cyclic biaxial behavior of concrete. They found that their model matched experimental results better than previous models (16, 18, 21). Romstad et al (26) presented a numerical biaxial characterization for concrete, which derives constitutive relations in biaxial form, from a multi-linear approximation of the

compressive stress-strain behavior, the biaxial failure stress envelope and Poisson's ratio.

1.3 OBJECT AND SCOPE The object of this study is to develop a finite element model of non-homogeneous concrete, consisting of mortar and aggregate, for in-plane loading conditions. Linear elastic properties of aggregate and nonlinear properties of mortar are employed. Experimental strength criteria are used to represent the mortar-aggregate interface. Experimental results (19) for monotonic biaxial loading and biaxial strength of mortar are combined with a previously developed numerical procedure (7) to represent nonlinear mortar.

The finite element study considers the simplified model of concrete suggested by Shah and Winter (28). Formation and propagation of interfacial and mortar cracks, and the load-deflection behavior of concrete as affected by the strength of the interface and linear and nonlinear representations of mortar are studied. The analytical load-deflection behavior of concrete is compared with the experimental results of Buyukozturk (2).

CHAPTER 2

MATERIAL MODEL

2.1 GENERAL Concrete is a non-homogeneous, inelastic material. It consists of aggregate, a material which is essentially linear and elastic (2, 11) and mortar, a nonlinear material (11, 19, 29). Both have different stiffness and strength characteristics. The bond between aggregate and mortar is the weakest link in the concrete system.

The purpose of the present investigation is to develop a finite element model of non-homogenous concrete. The analytical behavior of a material is related to the representation of its constituents. The prediction of the actual behavior requires the constitutive properties of the model to be based on the experimental characteristics. This necessitates separate representations of mortar, aggregate and the mortar-aggregate interface. The proposed model incorporates individual material characteristics in a simple model of concrete.

2.2 MORTAR

2.2.1. CONSTITUTIVE RELATION Mortar is modeled as an incrementally linear orthotropic material. The nonlinear behavior of the material is incorporated into the analysis by progressively updating the material properties as well as correcting the stresses and strains, as described in Chapter 3.

For the mortar model, the constitutive relations are defined along the principal stress axes. Changes of normal and shear stresses cause the principal and, therefore, material axes to rotate.

Following the work of Darwin and Pecknold (7), the incremental stress-strain relations in the material coordinates, 1-2, (See Eq. A .12, App. A) are given by

$$\begin{bmatrix} d\sigma_1 \\ d\sigma_2 \\ d\tau_{12} \end{bmatrix} = \frac{1}{1-\nu^2} \begin{bmatrix} E_1 & \nu\sqrt{E_1E_2} & 0 \\ & E_2 & 0 \\ \text{SYM} & & \frac{1}{4}(E_1+E_2-2\nu\sqrt{E_1E_2}) \end{bmatrix} \begin{bmatrix} d\varepsilon_1 \\ d\varepsilon_2 \\ d\gamma_{12} \end{bmatrix} \quad (2.1)$$

or $\{d\sigma\} = [D]\{d\varepsilon\}$

where E_1, E_2 are the tangent moduli of elasticity along the current principal stress axes, ν is the "effective" Poisson's ratio, and [D] is the constitutive matrix in the local (or material) coordinates.

The constitutive matrix in global coordinates, [D'], is obtained (Eq. A.10, App. A) by transforming [D] to the global coordinates. [D'] is used to calculate the element stiffness matrix.

Incremental changes in stress and strain, in the global coordinates, X-Y, are related as follows:

$$\begin{bmatrix} d\sigma_x \\ d\sigma_y \\ d\tau_{xy} \end{bmatrix} = \frac{1}{1-\nu^2} \begin{bmatrix} E_1\text{Cos}^2\theta+E_2\text{Sin}^2\theta & \nu\sqrt{E_1E_2} & \frac{1}{2}(E_1-E_2)\text{Cos}\theta\text{Sin}\theta \\ & E_1\text{Sin}^2\theta+E_2\text{Cos}^2\theta & \frac{1}{2}(E_1-E_2)\text{Cos}\theta\text{Sin}\theta \\ \text{SYM} & & \frac{1}{4}(E_1+E_2-2\nu\sqrt{E_1E_2}) \end{bmatrix} \begin{bmatrix} d\varepsilon_1 \\ d\varepsilon_2 \\ d\gamma_{12} \end{bmatrix} \quad (2.2)$$

where θ is the angle between material and global coordinate systems.

222 DETERMINATION OF INCREMENTAL MATERIAL PROPERTIES

The stress-strain relation for mortar in compression is nonlinear (11, 19, 29) and its behavior varies as a function of the ratio of

principal stresses. Mortar is represented using a numerical procedure, similar to the one developed by Darwin and Pecknold (7) for plain concrete. This procedure utilizes the concept of "equivalent uniaxial strain" which separates the Poisson's effect from the biaxial stress-strain curves. The stress-equivalent uniaxial strain curves, thus obtained, are used to keep track of the stress dependent variations in the material properties. The procedure is described below.

Equivalent Uniaxial Strain For an elastic material under biaxial stresses, the equivalent uniaxial strain in the ith principal direction, ε_{iu}, is the strain on the uniaxial stress-strain curve corresponding to the stress, σ_i. The actual strain in the ith direction, ε_i, corresponding to biaxial stresses, σ_i and σ_j, includes the Poisson effect.

$$\varepsilon_i = \frac{\sigma_i}{E} - \nu \frac{\sigma_j}{E} \tag{2.3}$$

where E = modulus of elasticity.

For the elastic material the equivalent uniaxial strain is given by

$$\varepsilon_{iu} = \frac{\sigma_i}{E} \tag{2.4}$$

For a nonlinear orthotropic material the differential change in equivalent uniaxial strain, $d\varepsilon_{iu}$, is given by

$$d\varepsilon_{iu} = \frac{d\sigma_i}{E_i} \tag{2.5}$$

where E_i is the tangent modulus of elasticity and $d\sigma_i$ is the differential change in stress along the ith direction. The total equivalent uniaxial strain, ε_{iu}, is obtained by integrating Eq. 2.5.

$$\varepsilon_{iu} = \int d\varepsilon_{iu} = \int \frac{d\sigma_i}{E_i} \tag{2.6.a}$$

In incremental form, Eq. 2.6.a becomes

$$\varepsilon_{iu} = \Sigma \Delta\varepsilon_{iu} = \sum_{\substack{\text{all} \\ \text{increments}}} \frac{\Delta\sigma_i}{E_i} \tag{2.6.b}$$

where $\Delta\varepsilon_{iu}$ is the incremental change in equivalent uniaxial strain corresponding to the incremental change in stress, $\Delta\sigma_i$.

The incremental changes in normal and shear stress cause rotation of the principal stress and, therefore, material axes. For material axes rotation, the incremental change in equivalent uniaxial strain is given by

$$\Delta\varepsilon_{iu} = \frac{\sigma_{inew} - \sigma_{iold}}{E_i} \tag{2.7}$$

where σ_{iold} is the total stress along the original i direction, before application of the load increment, E_i is the tangent modulus at the beginning of the increment, and σ_{inew} is the total stress along the new i direction after application of the load increment. ε_{iu} is obtained from Eq. 2.6.b, by adding $\Delta\varepsilon_{iu}$ to its previous value.

Stress vs Equivalent Uniaxial Strain Curves An equation given by Saenz (27) is used to represent stress vs equivalent uniaxial strain curves for different values of peak stress (Fig. 2.1).

$$\sigma_i = \frac{\varepsilon_{iu} E_o}{1 + [\frac{E_o}{E_s} - 2] \frac{\varepsilon_{iu}}{\varepsilon_{ic}} + (\frac{\varepsilon_{iu}}{\varepsilon_{ic}})^2} \tag{2.8}$$

where

E_o = tangent modulus of elasticity at zero stress,

E_s = secant modulus at the point of maximum stress, σ_{ic}

$= \frac{\sigma_{ic}}{\varepsilon_{ic}}$

ε_{ic} = equivalent uniaxial strain at maximum compressive stress, σ_{ic}

ε_{iu} = equivalent uniaxial strain at stress, σ_i

E_o, σ_{ic} and ε_{ic} are entered as independent variables in Eq. 2.8. E_o is obtained from experimental uniaxial stress-strain curves (19). Analytical expressions are used to determine σ_{ic} and ε_{ic}.

Biaxial Strength Envelope A simplified analytical biaxial strength envelope is developed for mortar based on experimental results of Liu (19). Both experimental and analytical envelopes are shown in Fig. 2.2. Taking tensile stress as positive (this sign convention is adopted throughout the report), the ratio between principal stresses, α, is given by

$$\alpha = \sigma_1/\sigma_2$$

where $\sigma_1 \geq \sigma_2$

The values of peak compressive stress, σ_{ic}, and peak tensile stress, σ_{it}, are obtained from the analytical envelope as described below ($i = 1,2$).

In Compression-Compression

For $\alpha < 0.2$

$$\sigma_{2c} = (0.4\ \alpha + 1)f'_c \tag{2.9}$$

$$\sigma_{1c} = \alpha\ \sigma_{2c}$$

$$= \alpha(0.4\ \alpha + 1)\ f'_c \tag{2.10}$$

where f'_c = uniaxial compressive strength

For $\alpha \geq 0.2$

$$\sigma_{2c} = 1.08\ f'_c \tag{2.11.a}$$

$$\sigma_{1c} = \alpha\ \sigma_{2c} \tag{2.11.b}$$

In Compression-Tension

$$\sigma_{1t} = f'_t \tag{2.12.a}$$

where f'_t = uniaxial tensile strength

$$\sigma_{2c} = f'_c \tag{2.12.b}$$

In tension-Tension

$$\sigma_{1t} = f'_t \tag{2.13.a}$$

$$\sigma_{2t} = f'_t \tag{2.13.b}$$

Equivalent Uniaxial Strain at Maximum Stress, ε_{ic}

Due to biaxial stress conditions, a specific reduction in the strain corresponding to the uniaxial stress is suggested for linear elastic materials, by Eq. 2.3. This full reduction is not demonstrated by the experimental results for mortar (19) which show an apparent increase in ductility for different combinations of biaxial stress. This increase in ductility is included in the mortar model. The equivalent uniaxial strain at maximum stress, ε_{ic}, is determined as follows:

The differential change in strain, $d\varepsilon_i$, corresponding to differential changes in principal stresses, $d\sigma_i$ and $d\sigma_j$, is given by

$$d\varepsilon_i = \frac{d\sigma_i}{E_i} - \nu_{ji}\frac{d\sigma_j}{E_j} \tag{2.14}$$

where E_i and E_j are the tangent moduli of elasticity and ν_{ji} is the Poisson's ratio, for an incrementally elastic orthotropic material.

For $\alpha = 1$ (equal biaxial compression)

$$d\sigma_i = d\sigma_j$$

$$E_i = E_j$$

$$\nu_{ji} = \nu_{ij} = \nu$$

Therefore, Eq. 2.14 gives

$$d\varepsilon_i = \frac{d\sigma_i}{E_i}(1-\nu) \tag{2.15}$$

In this case the differential change in equivalent uniaxial strain, $d\varepsilon_{iu}$, is given by

$$d\varepsilon_{iu} = \frac{d\sigma_i}{E_i} = \frac{d\varepsilon_i}{(1-\nu)} \tag{2.16}$$

Integrating the left and right sides of Eq. 2.16, the value of equivalent uniaxial strain, ε_{ic}, corresponding to the actual strain, ε_{im}, at maximum stress, σ_{ic}, is obtained:

$$\varepsilon_{ic} = \frac{\varepsilon_{im}\ (\alpha=1)}{(1-\nu)} \tag{2.17}$$

Average values for mortar (19) are:

$$|\varepsilon_{im}\ \ (\alpha = 1)| = 0.0024$$

$$|\varepsilon_{cu}| = 0.0025$$

where ε_{cu} is the strain at the peak of the uniaxial curve.

For $\nu = 0.2$, from Eq. 2.17,

$$|\varepsilon_{ic}\ (\alpha=1)| = 0.003$$

Therefore, $|\varepsilon_{ic}\ (\alpha=1)| > |\varepsilon_{cu}|$

To model this apparent increase in ductility a linear variation of ε_{ic} is used:

$$\varepsilon_{ic} = \varepsilon_{cu} \left[\frac{\sigma_{ic}}{f'_c} R - (R-1)\right] \tag{2.18}$$

where

$$R = \frac{\frac{\varepsilon_{ic}(\alpha=1)}{\varepsilon_{cu}} - 1}{\frac{\sigma_{ic}(\alpha=1)}{f'_c} - 1} \tag{2.19}$$

Eq. 2.18 is used to obtain the maximum equivalent uniaxial strain, ε_{ic}, for maximum stress, σ_{ic}, greater than f'_c in absolute magnitude. Using the average experimental values (19) for mortar, Eq. 2.9 gives: R = 2.5.

For maximum stress, σ_{ic}, less than f'_c in absolute magnitude, the maximum equivalent uniaxial strain, ε_{ic}, is given by

$$\varepsilon_{ic} = \varepsilon_{cu} \left[-1.70\left(\frac{\sigma_{ic}}{f'_c}\right)^3 + 2.30\left(\frac{\sigma_{ic}}{f'_c}\right)^2 + 0.40\left(\frac{\sigma_{ic}}{f'_c}\right)\right] \tag{2.20}$$

Eq. 2.20 provides a reasonably close match with experimental data. For small values, ε_{ic} is adjusted to keep the ratio of $\frac{E_o}{E_s} \geq 2$ in Eq. 2.8. This allows the stress-strain curve to remain convex upward.

2.2.3 COMPARISON OF ANALYTICAL AND EXPERIMENTAL STRESS-STRAIN CURVES

Analytical and experimental (17) stress-strain curves for mortar in biaxial compression are shown in Figs. 2.3-2.6. The analytical stress-strain curves are obtained by using the stress vs equivalent uniaxial strain curves.

The analytical curves are reasonably close to the experimental curves. The analytical curves do not match the experimental curves as well, along the minor direction, as they do along the major direction but the overall match is quite satisfactory for the finite element model.

A more sophisticated model could be used, but only at a higher numerical cost.

2.2.4.a CRACKING When the principal stress exceeds the tensile strength of mortar a crack forms perpendicular to the direction of the principal stress. It is modeled by reducing E to zero along the principal stress direction; and the constitutive relation now becomes (in material coordinates):

$$\begin{bmatrix} d\sigma_1 \\ d\sigma_2 \\ d\tau_{12} \end{bmatrix} = \frac{1}{1-\nu^2} \begin{bmatrix} 0 & 0 & 0 \\ 0 & E_2 & 0 \\ 0 & 0 & E_2/4 \end{bmatrix} \begin{bmatrix} d\varepsilon_1 \\ d\varepsilon_2 \\ d\nu_{12} \end{bmatrix} \tag{2.21}$$

This relation is obtained from Eq. 2.1 by substituting $E_1 = 0$. When a crack is formed, the material coordinates are fixed.

2.2.4.b. CRUSHING When the principal stress in the mortar exceeds the compressive strength, crushing occurs. In this study, crushing signalled the ultimate strength of the model.

2.3. AGGREGATE

Stone is very nearly an elastic, brittle material. Its stress vs longitudinal strain curve is essentially linear up to failure as shown in Fig. 2.7. Its stress vs volumetric/lateral strain curves are also plotted in Fig. 2.7. In monotonic loading of normal concretes no fracture of the aggregate occurs because of the high strength of the stone (11). The fracture of aggregate commonly observed in test cylinders occurs only at strains well past the ultimate strength of the specimen.

Aggregate is modeled, therefore, as a linear, isotropic, elastic material. The constitutive relation is

$$\begin{bmatrix} \sigma_x \\ \sigma_y \\ \tau_{xy} \end{bmatrix} = \frac{E}{1-\nu^2} \begin{bmatrix} 1 & \nu & 0 \\ & 1 & 0 \\ \text{SYM} & & \frac{(1-\nu)}{2} \end{bmatrix} \begin{bmatrix} \varepsilon_x \\ \varepsilon_y \\ \gamma_{xy} \end{bmatrix} \tag{2.22}$$

2.4. MORTAR-AGGREGATE INTERFACE

2.4.1. PROPERTIES OF INTERFACE The properties of the interfacial bond between mortar and aggregate, may be summarized as follows:

1. The interface between mortar and aggregate is the weakest link in the composite concrete system (12).

2. The compression-shear bond strength of the interface can be represented by the Mohr-Coulomb envelope (33) and is a straight line, i.e.,

$$\tau_{max} = c - \sigma_n \tan \phi \tag{2.23}$$

where τ_{max} = shear strength of the interface

σ_n = normal stress at the interface

c = cohesion

ϕ = angle of internal friction

3. Cohesion and angle of internal friction are basic material properties and the shear strength of the interface can be determined for any interfacial inclination, provided c and ϕ are known.

4. When the unconfined strength of the interface is exceeded, the cohesive part of the compression-shear bond strength is lost and sliding is resisted, thereafter, only by friction (28).

5. When the tensile strength of the interface is exceeded, an open crack developes. No normal or shear stress can be carried by the cracked portion of the interface.

No experimental data is available on the tensile-shear strength of the interface.

2.4.2. CONSTITUTIVE RELATION In the finite-element analysis the mortar-aggregate interface is modeled by so called "interfacial" elements (2). The interfacial element simulates the properties of the interfacial bond. The constitutive matrix to be described does not represent the properties of a physically existent material.

Assuming the "interfacial-material" to be elastic, its constitutive relation, in a coordinate system, 1-2, oriented parallel and perpendicular to the interface, is given as

$$\begin{bmatrix} d\sigma_1 \\ d\sigma_2 \\ d\tau_{12} \end{bmatrix} = \frac{1}{1-\nu^2} \begin{bmatrix} E & E & 0 \\ & E & 0 \\ SYM & & (1-\nu^2)G \end{bmatrix} \begin{bmatrix} d\varepsilon_1 \\ d\varepsilon_2 \\ d\nu_{12} \end{bmatrix} \qquad (2.24)$$

where E = modulus of elasticity (normally taken as the initial tangent modulus of mortar)

and G = shear modulus

$= \frac{E}{2(1+\nu)}$, for an uncracked interface.

2.4.3. STRENGTH The Mohr-Coulomb envelope has been adapted to model the strength of the interface for both compression-shear and tensile-shear types of failures of bond, as shown in Fig. 2.8. A splitting failure is assumed when the tensile strength is exceeded.

2.4.4. CRACKING

(a) Compression-Shear Cracking The Mohr-Coulomb envelope, in compression shear, assumes failure of bond, when

$$\tau \geq \tau'_{max}$$

where τ = shear stress at the interface

and τ'_{max} = shear strength of the interface

$= \tau_{max}$ (obtained in Eq. 2.23)

A crack is formed tangential to the interface and the constitutive relation in local coordinates becomes

$$\begin{bmatrix} d\sigma_1 \\ d\sigma_2 \\ d\tau_{12} \end{bmatrix} = \frac{1}{1-\nu^2} \begin{bmatrix} E & \nu E & 0 \\ & E & 0 \\ SYM & & (1-\nu^2)kG \end{bmatrix} \begin{bmatrix} d\varepsilon_1 \\ d\varepsilon_2 \\ d\nu_{12} \end{bmatrix} \qquad (2.25)$$

where kG is a small fraction of G

Resistance to sliding is offered only by friction and the new shear strength, τ''_{max}, is given by

$$\tau''_{max} = -\sigma_n \tan \phi \qquad (2.26.a)$$

It is assumed that the sliding does not stop, i.e.,

$$\tau = \tau_{max} \qquad (2.26.b)$$

The apparent change in shear stress (Eq. 2.25) gives an apparent total stress which is corrected to τ''_{max} using Eq. 2.26 as described in Chapter 3.

If the normal stress becomes zero or positive, the crack opens and no normal or shear stresses can be transferred across the interface. The constitutive relation in local coordinates, becomes

$$\begin{bmatrix} d\sigma_1 \\ d\sigma_2 \\ d\tau_{12} \end{bmatrix} = \frac{1}{1-\nu^2} \begin{bmatrix} E & 0 & 0 \\ & 0 & 0 \\ SYM & & 0 \end{bmatrix} \begin{bmatrix} d\varepsilon_1 \\ d\varepsilon_2 \\ d\nu_{12} \end{bmatrix} \qquad (2.27)$$

(b) Tensile/Tensile-Shear Cracking: In tension-shear, when,

$$\tau \geq \tau'_{max} \quad \text{(Mohr-Coulomb envelope)}$$

the interface loses its capacity to carry any normal or shear stresses.

$$\therefore \quad \tau''_{max} = 0 \tag{2.28}$$

An open crack is formed and the constitutive relation takes the form of Eq. 2.27.

CHAPTER 3

FINITE ELEMENT ANALYSIS

3.1 ISOPARAMETRIC ELEMENT The finite element used in this study is a four-noded quadrilateral isoparametric element with two degrees of freedom at each node. The element has straight sides but is otherwise of arbitrary shape. The element and the "parent" rectangular element are shown in Fig. B.1. It is formulated using an intrinsic coordinate system, which is defined by element geometry, not by the element-orientation in the global coordinate system. The element is "invariant" (properties independent of orientation), if it is uniformly integrated. It gives satisfactory results for states of uniform normal loading and pure shear but it behaves badly under pure bending. "Parasitic" shear is introduced by bending. In the present analysis normal and shear stresses predominate and the problem of bending is minor.

The element stiffness matrix is calculated using the Gaussian numerical integration technique. The element needs only one Gauss point for satisfactory integration but in order to follow the nonlinear behavior of the material and to allow variation in the state of the material across the element, a two-by-two Gauss rule is adopted.

Element properties are presented in greater detail in Appendix B.

3.2 ANALYSIS PROCEDURE

3.2.1 GENERAL The input for the analysis consists of the specification of the topology of the structure and the properties of the constituent materials. The properties of aggregate, mortar and the mortar-aggregate

interface are specified. Because aggregate is modeled as a linear elastic material, its properties remain constant throughout the analysis. The properties of finite elements representing the mortar-aggregate interface change only after cracking of the interface. The properties of mortar vary from point to point and with loading.

A stepwise, incremental procedure is adopted to trace the path-dependent behavior of concrete, caused by irreversible microcracking and the nonlinearity of mortar under compression.

For the first increment, the virgin constitutive properties of the material are used to obtain the stiffness of the structure. Incremental loads, either in the form of nodal loads or prescribed nodal displacements are applied. The resulting incremental displacements are used to calculate apparent changes in stress. The "actual" changes in stress are obtained through the material model. Corrective (or residual) nodal loads are obtained by comparing the apparent stresses with those predicted by the model. An Adaptation of the Initial Stress Method with Variable Stiffness (7) is used for this purpose and is illustrated schematically in Fig. 3.1. The updated constitutive properties of the material are used to obtain new element stiffnesses, which are assembled to form the new structure stiffness. The residual loads are re-applied in the next iteration using the updated structure stiffness. The correction of stresses and loads is continued until specific convergence criteria (Section 3.3) are obtained at which point the next increment of load is applied. Each increment, contains a number of iterations as each new incremental load is applied. Residual loads remaining from the previous iteration are added.

3.2.2 ITERATIVE SOLUTION The solution procedure is described in more

detail as follows:

For the ith iteration of a load increment, the constitutive matrix of nth element, updated at the end of the previous iteration, is $D^{(i-1)}$. The element stiffness is

$$k_n^{(i-1)} = \int_v B^T D^{(i-1)} B dV \tag{3.1}$$

where B is the strain-displacement relationship matrix (See Appendix B.). The structure stiffness, $K^{(i-1)}$, is obtained by assembling the element stiffnesses and is given by

$$K^{(i-1)} = \sum_n L_n K_n^{(i-1)} \tag{3.2}$$

where L_n = matrix for transforming local displacements to the global coordinates.

The equilibrium equations, give

$$K^{(i-1)} \delta U^{(i)} = \delta P^{(i-1)} \tag{3.3}$$

Therefore,

$$\delta U^{(i)} = K^{(i-1)|^{-1}} \delta P^{(i-1)} \tag{3.4}$$

where $\delta P^{(i-1)}$ = nodal loads

and $\delta U^{(i)}$ = nodal displacements.

In general, the nodal loads, $\delta P^{(i-1)}$, represent both applied loads (known) and reactions (unknown), while the displacements, $\delta U^{(i)}$, are both prescribed (e.g. at the boundaries) or unknown. The element nodal displacements, $\delta u^{(i)}$, are obtained from structure nodal displacements, $\delta U^{(i)}$ (Eq. 3.4).

For each element, n, the change in material strains, $\delta\varepsilon^{(i)}$, and the apparent change in material stresses, $\delta\sigma^{(i)}$, are obtained in Eqns. 3.5 and 3.6.

$$\delta\varepsilon^{(i)} = B\delta u^{(i)} \tag{3.5}$$

$$\delta\sigma^{(i)} = D^{(i-1)}\ \delta\varepsilon^{(i)} \tag{3.6}$$

The "actual" changes in stress, $\Delta\sigma^{(i)}$, and the updated constitutive matrices, $D^{(i)}$, are obtained from the material model

$$\Delta\sigma^{(i)} = \Delta\sigma^{(i)}\ (\sigma^{(i-1)},\ \delta\sigma^{(i)},\ \varepsilon^{(i-1)},\ \delta\varepsilon^{(i)}, \ldots) \tag{3.7.a}$$

$$D^{(i)} = D^{(i)}\ (\sigma^{(i-1)},\ \delta\sigma^{(i)},\ \varepsilon^{(i-1)},\ \delta\varepsilon^{(i)},\ \ldots) \tag{3.7.b}$$

These constitutive relations, Eqs. 3.7, are described in Chapter 2.

The total stress, $\sigma^{(i)}$, in the element is given by

$$\sigma^{(i)} = \sigma^{(i-1)} + \Delta\sigma^{(i)} \tag{3.8}$$

The element residual stresses, $\sigma_R^{(i)}$, are obtained by taking the difference,

$$\sigma_R^{(i)} = \delta\sigma^{(i)} - \Delta\sigma^{(i)} \tag{3.9}$$

Residual loads are then generated for the structure

$$R^{(i)} = \sum_n \int_V B^T \sigma_R^{(i)} dV \tag{3.10}$$

The nodal loads, for the next iteration are

$$\delta P^{(i)} = \Delta P^{(i)} + R^{(i)} \tag{3.11}$$

The new structure stiffness, $K^{(i)}$, is obtained using Eqs. 3.1 and 3.2 and the updated constitutive matrices, $D^{(i)}$.

If the convergence criteria are satisfied, a new load increment, $\Delta P^{(i)}$, is applied and iterations are restarted for this new increment. If convergence is not obtained, the $(i+1)$th iteration is carried out. For this iteration, the incremental load is the residual load from the previous iteration, i.e.,

$$\Delta P^{(i)} = 0$$

and

$$\delta P^{(i)} = R^{(i)}$$

3.2.3 SOLUTION OF EQUILIBRIUM EQUATIONS In general a portion of the nodal loads, as well as the nodal displacements, are prescribed in Eq. 3.3. Using the subscript "I" to denote the "interior" nodes (i.e., the nodes at which loads are specified) and the subscript "B" to denote the "boundary" nodes (i.e., the "exterior" nodes at which displacements are specified) the equilibrium equations may be written in partitioned form as,

$$\begin{bmatrix} K_{II}^{(i-1)} & K_{IB}^{(i-1)} \\ K_{BI}^{(i-1)} & K_{BB}^{(i-1)} \end{bmatrix} \begin{bmatrix} \delta U_I^{(i)} \\ \delta U_B^{(i)} \end{bmatrix} = \begin{bmatrix} \delta P_I^{(i-1)} \\ \delta P_B^{(i-1)} \end{bmatrix} \tag{3.12}$$

Incorporating the known quantities, Eq. 3.12 is altered:

$$\begin{bmatrix} K_{II}^{(i-1)} & 0 \\ 0 & I \end{bmatrix} \begin{bmatrix} \delta U_I^{(i)} \\ \delta U_B^{(i)} \end{bmatrix} = \begin{bmatrix} \delta \bar{P}_I^{(i-1)} - K_{IB}^{(i-1)} \delta \bar{U}_B^{(i)} \\ \delta \bar{U}_B^{(i)} \end{bmatrix} \tag{3.13}$$

where the overbars indicate the prescribed values in Eq. 3.13.

For the first iteration, i = 1

$$\delta\bar{P}_I^{(0)} = \Delta P_I + R_I$$
$$\delta\bar{U}_B^{(1)} = \Delta\bar{U}_B \tag{3.14}$$

where ΔP_I and $\Delta\bar{U}_B$ are the increments of interior nodal loads and boundary nodal displacements.

For subsequent iterations, i > 1

$$\delta\bar{P}_I^{(i-1)} = R_I^{(i-1)}$$
$$\delta\bar{U}_B^{(i)} = 0 \tag{3.15}$$

In practice, the partitioning shown in Eq. 3.13 is not done, as it would greatly increase the band width of the stiffness matrix. The stiffness terms corresponding to the known displacements are saved in auxiliary storage. The rows and columns of the stiffness matrix corresponding to the known displacements are, then, made equal to zero, except the diagonal terms which are made equal to unity. The load vector is changed appropriately, as shown in Eq. 3.13.

The reactions associated with boundary displacements, $\delta P_B^{(i-1)}$, are calculated using the information in auxiliary storage. Therefore, from Eq. 3.12

$$\delta P_B^{(i-1)} = K_{BI}^{(i-1)}\ \delta U_I^{(i)} + K_{BB}^{(i-1)}\ \delta U_B^{(i)} \tag{3.16}$$

The residual loads, $R_B^{(i)}$, are calculated using Eq. 3.10.

The nodal load increment, ΔP_B, at the boundary nodes, is given by (for any number of iterations, i)

$$\Delta P_B = \delta P_B^{(0)} - R_B^{(1)} + \delta P_B^{(1)} - R_B^{(2)} + \ldots + \delta P_B^{(i-1)} - \delta R_B^{(i)} \quad (3.17)$$

3.3 CONVERGENCE CRITERIA Two criteria are used to establish convergence for an increment of load, one based on displacement and the other upon the magnitude of the residual loads.

(1) Displacement Criteria: The square root of the sum of the squares (root sum squares or RSS) of the change in nodal displacements for the last iteration, $\delta U^{(i)}$, is compared to the RSS of the total nodal displacements, U, and to the RSS of the change in the displacements occurring since the last load increment, ΔU. If the RSS for the latest changes is smaller than one-hundredth of the RSS of the total displacements or one-twentieth of the RSS of the total change in displacements, the solution is considered to have converged. These criteria are expressed symbolically as follows:

$$\frac{RSS(\delta U^{(n)})}{RSS(U)} \leq \frac{1}{100} \text{ or } \frac{RSS(\delta U^{(n)})}{RSS(\Delta U)} \leq \frac{1}{20}$$

where

$$RSS(a) = (\sum_i a_i^2)^{\frac{1}{2}}$$

Once the displacement criteria are met, the solution is then checked for force convergence.

(2) Force Criterion: The residual load at each node is checked. The residual load at each node is compared with one-fiftieth of the largest

total calculated nodal load (both of them in absolute magnitude).

Symbolically

$$\frac{|R_i|}{|P_{max}|} \leq \frac{1}{50} \text{ , } i = 1, \text{ structure degrees of freedom}$$

R_i = residual load for structure degree of freedom, i

P_{max} = maximum total nodal load.

CHAPTER 4

NUMERICAL STUDY

4.1 GENERAL The material and finite element representations presented in Chapters 2 and 3 are combined to model plain concrete using Shah and Winter's (28) simple "Structural Unit" (Fig. 4.1). Because of the symmetrical shape only one quarter of the unit is analyzed. The finite element model is shown in Fig. 4.2. Incremental boundary displacements are applied and the corresponding boundary loads determined in the analysis. For uniaxial loading, the lateral displacement is measured at midheight of the vertical boundary (i.e., lower right corner of the finite element model).

The model is used to investigate the importance of mortar-aggregate interfacial strength and mortar nonlinearity on the behavior of concrete under uniaxial compressive loading. Behavior of the model under biaxial compressive stresses is also investigated.

Limited comparisons are made to the more complicated physical and analytical models of Buyukozturk (2). Each analysis is terminated upon initiation of crushing in the mortar.

4.2. PLAN OF STUDY

4.2.1 MATERIAL PROPERTIES The material properties used in the finite element analysis are given below:

(1) Interface: (a) Cohesion = 300 psi, (b) tensile strength = 411 psi, (c) angle of internal friction = 36^{o}

(2) Aggregate, (a) $E = 5.0 \times 10^{6}$ psi, (b) $\nu = 0.26$

(3) Mortar = (a) $E_i = 2.8 \times 10^{6}$ psi, (b) $\nu = 0.2$, (c) $f'_m = 3300$ psi,

(d) ε_{cu} = 0.0025 in/in, (e) tensile strength = 350 psi,

where E = modulus of elasticity and subscript i indicates its initial value,

ν = Poisson's ratio,

and ε_{cu} = strain corresponding to maximum unaixial stress, f'_m

The above values are average experimental (2, 14, 19, 33) values, except for the tensile strength of interfacial bond which is obtained by extending the Mohr-Coulomb envelope from compression-shear zone to the tensile-shear zone.

4.2.2 POINTS OF STUDY The following points were studied using the finite element model:

Uniaxial Compressive Loading

(1) Formation and Propagation of interfacial cracks,

(2) Formation and Propagation of mortar cracks,

(3) Load-Deflection Behavior of concrete,

(4) Strength of Concrete as affected by,

(a) Strength of interface:

Case I: Infinite bond strength

Case II: Normal bond strength

Case III: Zero tensile and cohesive strength

Case IV: Zero bond strength (Case III plus zero angle of internal friction)

(b) Representation of mortar

(i) Linear,

(ii) Nonlinear

(c) Relative proportions of aggregate and mortar:

(i) d/r = 2/3

(ii) d/r = 1/2 (for case b.ii only)

(where r = radius of aggregate disc and d = minimum thickness of mortar, see Fig. 4.1)

Biaxial Compressive Loading

(1) Load-deflection behavior

(2) Strength

as affected by:

(a) Representation of mortar

(i) Linear (biaxial strength taken equal to uniaxial strength)

(ii) Nonlinear (analytical biaxial behavior employed)

(b) Relative proportions of aggregate and mortar:

(i) d/r = 2/3

(ii) d/r = 1/2

Ratios of biaxial stresses and strains:

(1) Ratio of principal strains = 1:1

(corresponding ratio of principal stresses = 1:1)

(2) Ratio of principal strains = 1:2

(corresponding ratio of principal stresses ~.64:1 to .67:1).

4.3 RESULTS AND DISCUSSION

4.3.1 UNIAXIAL COMPRESSIVE LOADING

CASE I: Normal (Experimental) Interfacial Strength: For the interfacial properties listed in Section 4.2.1 and d/r = 2/3, stress-strain curves for the model are shown in Fig. 4.3. Both linear and nonlinear representations for mortar are used.

The discontinuities on the load-deflection curves represent extensive bond and mortar cracking. The stress-strain curve for the model with linear mortar is almost linear up to failure with a single change of slope at the discontinuity. For the nonlinear mortar, the curve is highly nonlinear. Nonlinearity begins at about 35% of the ultimate strength. This suggests that the nonlinearity is caused essentially by the nonlinear behavior of mortar in compression. Cracking patterns are compared using Fig. 4.4 and Table 4.1. The cracking patterns observed are similar and can, therefore, be represented by a single set of figures. The stresses and strains at which the various stages in cracking are observed differ, as can be seen in Table 4.1. Bond cracking starts at about 41% of ultimate strength for the model with linear mortar. The lower half of the interface is cracked, out of which the lower third is due to tensile-shear failure and the remaining is due to compression-shear failure. Mortar cracking begins at about 79% and 74% of ultimate strength for the cases of linear and nonlinear mortar representations, respectively. Experimental results indicate that mortar cracking is initiated at about 70-80% of the ultimate strength of concrete. This suggests that the behavior of the model is similar to the experimental behavior of concrete. Mortar cracking is initiated at the tip of the bond crack, and at higher loads most of the cracks start at the cracked interfacial boundary except for the mortar cracking on the top of the aggregate. There is only

limited mortar cracking in the case of linear mortar, whereas for the nonlinear mortar, a large increase in mortar cracking is observed, at about 94% of the ultimate strength of the model. The ultimate strength of the model, with linear mortar is 88% of the uniaxial mortar strength and with nonlinear mortar 90% of the uniaxial mortar strength.

CASE II: Infinite Interfacial Strength: Stress-strain curves with linear and nonlinear representations of mortar are shown in Fig. 4.5. The stress-strain curve for the model with linear mortar remains elastic up to failure, while the curve with nonlinear mortar begins to deviate from linearity at about the same load as in Case I. Because of the infinite strength of the interface, no bond cracks occur. No mortar cracks are formed for either the linear or the nonlinear representations of mortar. These results combined with Case I, confirm to at least a limited entent the experimental work (12) that indicated that mortar cracks are initiated by bond cracks. The increase in strength of model is only about 3% for linear mortar and about 4% for nonlinear mortar, compared to the strength of model with normal interfacial strength. This seems to indicate that very little additional strength can be gained by increasing the mortar-aggregate bond strength.

CASE III: Zero tensile and Cohesive Interfacial Strength. The stress-strain curves for linear and nonlinear representations of mortar are shown in Fig. 4.6. These curves represent the behavior of the model with no tensile or cohesive interfacial

strength. Friction at the interface remains equal to its normal value. The curve for the model with the linear mortar remains linear, whereas the curve for the model with nonlinear mortar begins to deviate from linearity at the same load as in the previous two cases. Bond cracking occurs as loading begins. This simulates the presence of interfacial cracks before loading. The lower two thirds of the interface cracks due to compression shear type of failure, out of which the lower half changes from the compression-shear to the tensile-shear type of cracking. (Table 4.2 and Fig. 4.7). As in Case I, mortar cracking is initiated at the tip of bond crack. The pattern of cracking is similar to that in Case I. Limited mortar cracking is observed in the case of linear mortar representation. These results suggest that whether bond cracking occurs prior to or after loading, the pattern of crack propagation remains essentially the same. The reduction in strength due to zero tensile and cohesive strength of interface is about 2% for both linear and nonlinear representations of mortar. This seems to confirm the experimental work by Darwin and Slate (6), who in contradiction to two other studies (4, 30), found that the reduction in bond strength of the interface between mortar and aggregate has a small effect on the strength of Portland Cement Concrete.

CASE IV: Zero Interfacial Strength: In this case, in addition to zero cohesive and tensile strength, the angle of internal friction is also made equal to zero. This case investigates

the extreme case of frictionless contact between aggregate and mortar. With the application of load, mortar begins to slide down the frictionless curved surface of aggregate at the very beginning of the stress-strain curve. The lower two-thirds of the interface changes from compression-shear to tensile-shear type of failure. Mortar cracking begins at the top of mortar-aggregate interfacial boundary at a stress equal to 532 psi in the case of linear mortar and 521 psi in the case of nonlinear mortar.

For the model with linear mortar, the stress-strain curve is multi-linear with different slopes before and after the mortar cracking (Fig. 4.8). The ultimate strength is 61% of the model with normal interfacial strength. Failure occurs due to crushing at the base of the finite element model.

For nonlinear mortar, the stress-strain curve is highly non-linear, particularly for the lateral strain, which is almost twice as large as longitudinal strain near the peak of the curve (Fig. 4.8). The large discontinuity in the lateral strain curve occurs at the initiation of mortar cracks. The reduction in strength is about 23% as compared to the strength of the model with normal interfacial strength. This result again points out the surprisingly small role played by interfacial strength on the behavior of the model and perhaps, concrete. The behavior of mortar appears to be of dominant importance.

The cracking patterns are described in Table 4.3 and Fig. 4.9. For both linear and nonlinear mortar, cracking of mortar is gradual and begins along the cracked interfacial boundary. The pattern of

crack propagation is similar to that observed in Case I and Case III.

DIFFERENT PROPORTIONS OF MORTAR AND AGGREGATE: Fig. 4.10 shows stress-strain curves for the model with d/r = 2/3 and d/r = 1/2. In both of these cases, a nonlinear mortar and normal interfacial strength are employed. The increased amount of aggregate increases the initial stiffness from 3.1×10^6 psi for d/r = 2/3 to 3.3×10^6 psi for d/r = 1/2. The increased volume of aggregate and/or the larger radius of aggregate disc decreases the strength of the model by about 2% for d/r = 1/2 compared to the strength of the model with d/r = 2/3. Comparison of initiation and propagation of cracks is described in Table 4.1 and Fig. 4.5. Bond cracking starts at about 44% of ultimate strength in both cases. Mortar cracking begins at about 61% of ultimate strength for d/r = 1/2 and 74% of ultimate strength for d/r = 2/3. Experimental results (12) indicate that mortar cracks begin to propagate and spread at about 70-90% of the ultimate strength of concrete. Thus, the behavior of the model is close to the experimental behavior of concrete.

4.3.2 COMPARISON OF ANALYTICAL AND EXPERIMENTAL UNIAXIAL LOADING CURVES

The analytical uniaxial curve with nonlinear representation of mortar and normal interfacial strength is compared with Buyukozturk's (2) experimental and analytical curves as shown in Fig. 4.11.

Buyukozturk used a similar but more complicated model of concrete for both experimental and analytical study, consisting of nine discs of aggregate embedded in a mortar matrix as shown in Fig. 4.12. The multiplicity of aggregate particles and the resulting mutual confinement of mortar and aggregate is a basic property of concrete. Buyukozturk's model is closer to real concrete because it incorporates

the multiplicity of aggregate discs in the mortar matrix. The simplified model used in the present study lacks mutual confinement of mortar and aggregate because it consists of single disc of aggregate embedded in a mortar matrix. Buyukozturk's model was not studied in the present investigation because of the high cost of numerical analysis for this particular case.

Compared to the simple analytical model, the experimental curve is initially stiffer. It fails at a higher load but at a comparable strain. The shape of the analytical curve is similar to the experimental curve. Buyukozturk's analytical representation models the geometry of this physical model, but employs an elastic representation of mortar. Apparently, to make his model look softer and allow a larger strain at failure, he used a modulus of elasticity for mortar equal to the secant modulus at about fifty percent of the experimental uniaxial strength and a mortar strength about 1.2 times the experimental uniaxial strength. His analytical stress-strain curve is almost linear up to failure except for a discontinuity at the initiation of bond cracks. The curve does not have any discontinuity corresponding to mortar cracking. This may be partly due to confinement in the more complicated system of Buyukozturk's model, which limits displacements after cracking.

4.3.3 COMPARISON OF STRESS-STRAIN CURVES OF THE MODEL WITH DIFFERENT INTERFACIAL STRENGTHS Stress-strain curves for the model with different interfacial strengths are compared in Fig. 4.13 for linear mortar and in Fig. 4.14 for nonlinear mortar. The curves show that the cohesive and tensile strengths of interface have a small effect on the behavior of concrete, whereas the angle of internal friction has a significant effect.

The effect on strength for the linear mortar is quite major. In all cases cracking causes discontinuities in the stress-strain curve, larger in the lateral direction than in the longitudinal direction. This effect is most pronounced in the case of the model with the frictionless interface. For all variations in interfacial strength, the stress-strain curves of the model with linear mortar remain almost linear to failure. The discontinuity due to cracking only changes the slope of the curve slightly. The stress-strain curves of the model with nonlinear mortar are nonlinear in all cases.

4.3.4 BIAXIAL LOADING The biaxial behavior of the model is obtained, for (1) d/r = 2/3 and (2) d/r = 1/2, with (a) linear mortar (biaxial strength taken equal to its uniaxial strength), for d/r = 2/3 only and with (b) nonlinear mortar (analytical behavior employed), and compared to experimental (2) behavior in Figures 4.15, 4.16 and 4.17.

Biaxial Stress-Strain Curves: The stress-strain curves for the model employing a linear representation of mortar are linear up to failure since no cracking occurs. With nonlinear mortar, the stress-strain curves are highly nonlinear (Fig. 4.15). The curves for biaxial compression are stiffer than the uniaxial curves and the biaxial strength is greater than the uniaxial strength of the model for both linear and nonlinear mortar representations. The stress-strain curves for the model with d/r = 2/3 and nonlinear mortar are compared with experimental curves for ratio of biaxial stresses equal to 1 (Fig. 4.16). The experimental and analytical curves have similar shape, but the experimental curve is initially stiffer and fails at a higher load. The higher initial stiffness may be due to the higher percent of aggregate in the

experimental model. The difference between experimental and analytical strengths is of the same order of magnitude as that obtained for uniaxial compression.

Biaxial Strength Envelope: In the case of both linear and nonlinear representations of mortar, the ratio between biaxial and uniaxial strength of the model is larger than the ratio between biaxial and uniaxial strengths of mortar. This suggests that the improvement in biaxial strength is the result of improved stress fields due to the biaxial compression. Not only is cracking suppressed but local compressive stresses in the mortar are reduced. The improved stress fields are best illustrated by the model with linear mortar which showed an increase in strength as high as seven percent, although the linear mortar itself has a biaxial strength equal to its uniaxial strength.

The analytical biaxial strength envelopes are compared to the experimental envelope obtained by Buyukozturk, in Fig. 4.17. The analytical strength envelopes are based on three ratios of principal stress (i.e., for $\alpha = 0$, $\alpha \sim 0.64$ to 0.67, and $\alpha = 1$). The analytical strength envelope with $d/r = 0.5$, which corresponds to the value in Buyukozturk's experimental model, has a shape and magnitude similar to the experimental biaxial strength envelope.

CHAPTER 5

SUMMARY AND CONCLUSIONS

5.1 SUMMARY A finite element model of concrete is developed to study the strength and deformation of plain concrete as a nonhomogeneous material under uniaxial and biaxial compressive stresses. Separate representations for mortar, aggregate and the mortar-aggregate interface based on experimental characteristics are employed. Aggregate is represented as an elastic material. A Mohr-Coulomb strength envelope is used to represent the bond strength of the mortar-aggregate interface. The nonlinear behavior of mortar is modeled by taking into account its behavior under different combinations of biaxial stress. The analytical stress-strain curves for mortar in compression are compared with experimental curves (19).

A stepwise, incremental procedure is used to trace the path dependent behavior of concrete, caused by irreversible microcracking and the nonlinearity of mortar in compression.

The study uses a highly simplified model of concrete. Formation and propagation of interfacial and mortar cracks and load-deflection behavior, are studied, as affected by interfacial strength, linear/nonlinear representations for the mortar constituent, and relative proportions of aggregate and mortar. For biaxial loading, the effects of linear/nonlinear mortar and relative proportions of aggregate and mortar, on the strength and the stress-strain behavior of concrete are studied.

5.2. CONCLUSIONS

(1) The finite element model of concrete, using a nonlinear representation of mortar and experimental interfacial strength criteria,

closely matches the overall uniaxial and biaxial behavior of a similar experimental model.

(2) The effect of the tensile and cohesive strength of the mortar-aggregate interface on the behavior of the model of concrete is small compared with the effect of nonlinearity of mortar; the effect of the friction between mortar and aggregate is of greater significance but still has less effect than the mortar in controlling the behavior of the model.

(3) In the model, mortar cracks are initiated only in the presence of bond-cracks. If there is no bond-cracking, no mortar cracking occurs. The pattern of crack propagation is similar whether cracks are present at the interface before loading or are caused by loading.

(4) A large amount of mortar cracking occurs prior to failure for the model with nonlinear mortar. Crushing occurs with a smaller amount of mortar cracking for the model with linear mortar.

(5) The effect of interfacial bond strength on the uniaxial strength of the model is small. This seems to confirm the experimental results of Darwin and Slate (6).

(6) The biaxial strength envelope for the nonlinear model is similar in shape and magnitude to experimental biaxial strength envelopes.

(7) The model study indicates that improved stress fields under biaxial compression cause an increase in strength. The increase (up to 19%) in the biaxial strength is larger than, can be attributed to the increase in mortar strength at the same stress ratio.

5.3 RECOMMENDATIONS FOR FUTURE STUDY

(1) The nonlinearity caused by removing friction between aggregate

and mortar is relatively large. This may be due to lack of confinement of mortar in the simplified model of concrete studied. The effect of confinement of mortar should be studied using Buyukozturk's (2) model of concrete.

(2) The mortar-aggregate interface of the model was represented by a layer of finite elements. In place of the "finite thickness" approach for the interface, other, more realistic representations should be investigated. Due to lack of experimental data, the tensile strength of mortar was constant in the model. The behavior of mortar in tension-compression should be investigated experimentally and a better representation of the strength envelope for mortar used in this region.

(3) The multiplicity of aggregate particles and their random distribution is a basic property of concrete. The effect of multiplicity of aggregate particles on the load-deflection behavior of the model needs to be studied.

(4) The variation in the shape of aggregate should also be studied in connection with (3).

(5) This study neglects the descending portion of the mortar stress-strain curve. The effect of this aspect of mortar behavior on the load-deflection and microscopic behavior of concrete should be investigated.

REFERENCES

1. Ash, J. E., "Bleeding in Concrete--A Microscopic Study," J. ACI, Proc. V. 69, n. 4, April, 1972, p. 209-211.

2. Buyukozturk, O., "Stress-Strain Response and Fracture of a Model of Concrete in Biaxial Loading," Ph.D. Thesis, Faculty of Graduate School, Cornell University, June, 1970.

3. Carino, N. J., and Slate, F. O., "Limiting Tensile Strain Criterion for failure of Concrete," J. ACI, Proc. V. 73, n. 3, Mar. 1976, p. 160-165.

4. Christensen, P. N., and Neilsen, T. P. H., "Model Determination of the Effect of Bond Between Coarse Aggregate and Mortar on the Compressive Strength of Concrete," J. ACI, Proc. V. 66, n. 1, Jan. 1969, p. 69-72.

5. Cook, R. D., Concepts and Applications of Finite Element Analysis, John Wiley and Sons, Inc., New York, 1974.

6. Darwin, D. and Slate, F. O., "Effect of Paste-Aggregate Bond Strength on Behavior of Concrete," Journal of Materials, JMLSA, V. 5, n. 1, Mar. 1970, p. 86-98.

7. Darwin, D. and Pecknold, D. A. W., "Inelastic Model for Cyclic Biaxial Loading of Reinforced Concrete," SRS n. 409, Civil Engr. Dept. University of Illinois, Urbana, Illinois, July, 1976.

8. Darwin, D. and Pecknold, D. A. W., "Analysis of R. C. Shear Panels Under Cydlic Loading," J. Struct. Div., V. 102, n. ST2, Feb. 1976, p. 355-369.

9. Desayi, P. and Krishnan, S., "Equation for the Stress-Strain Curve of Concrete," J. ACI, Proc. V. 61, n. 3, Mar. 1964, p. 345-350.

10. Hognestad, E., Hanson, N. W., and McHenry, D., "Concrete Stress Distribution in Ultimate Strength Design, " J. ACI, Proc. V. 27 n. 4, Dec. 1955, p. 455-479.

11. Hobbs, D. W., "The Strength and Deformation of Concrete Under Short-Term Loading: A Review," Technical Report No. 42.484, Sept. 1973, Cement and Concrete Association, London.

12. Hsu, T. C., Slate, F. O., Sturman, G. M., and Winter, G., "Micro-cracking of Plain Concrete and the Shape of the Stress-Strain Curve," J. ACI, Proc. V. 60, n. 2, Feb. 1963, p. 209-224.

13. Hsu, T. C., "Mathematical Analysis of Shrinkage Stresses in a Model of Hardened Concrete," J. ACI, Proc. V. 60, n. 3, Mar. 1963, p. 371-390.

14. Hsu, T. C. and Slate, F. O., "Tensile Strength Between Aggregate and Cement Paste or Mortar," J. ACI, Proc. V. 60, n. 4, April, 1963, p. 465-486.

15. Hurley, D. M., "A Proposed Computer Model for the Study of Plain Concrete Behavior," M.S. Thesis, Cornell University, 1967.

16. Karsan, I. D., and Jirsa, J. O., "Behavior of Concrete Under Compressive Loadings," J. Struct. Div., ASCE, V. 95, n. ST12, Dec. 1969, p. 2543-2563.

17. Kupfer, H., Hilsdorf, H. K., and Rusch, H., "Behavior of Concrete Under Biaxial Stresses," J. ACI, Proc. V. 66, n. 2, Aug. 1969, p. 656, 666.

18. Kupfer, H. B. and Gerstle, K. H., "Behavior of Concrete Under Biaxial Stresses," J. Engr. Mech. Div., ASCE, V. 99, n. EM4, Aug. 1973, p. 852-866.

19. Liu, T. C. Y., "Stress-Strain Response and Fracture of Concrete in Biaxial Compression," Ph.D. Thesis and Research Report No. 339, Dept. of Struct. Engr. Cornell University, Ithaca, N. Y., Feb., 1971.

20. Liu, T. C. Y., Nilson, A. H., and Slate, F. O., "Stress-Strain Response and Fracture of Concrete in Uniaxial and Biaxial Compression," J. ACI, Proc. V. 69, n. 5, May, 1972, p. 291-295.

21. Liu, T. C. Y., Nilson, A. H., and Slate, F. O., "Biaxial Stress-Strain Relations for Concrete," J. Struct. Div., ASCE, V. 98, n. ST5, May, 1972, p. 1025-1034.

22. Meyers, B. L., Slate, F. O., and Winter, G., "Relationship between Time Dependent Deformation and Microcracking of Plain Concrete," J. ACI, Proc. V. 66, n. 1, Jan. 1969, p. 60-68.

23. Nelissen, L. J. M., "Biaxial Testing of Normal Concrete," Heron, Netherlands, V. 8, n. 1, 1972.

24. Niva, Y. and Kobayashi, S., "Failure Criterion of Cement Mortar Under Triaxial Compression," Memoirs, Faculty of Engr., Kyoto University, Japan, V. 29, 1976, p. 1-15.

25. Radjy, F. and Hansen, T. C., "Fracture of Hardened Cement Paste and Concrete," Cem. Conc. Res., V. 3, n. 4, July, 1973, p. 343-361.

26. Romstad, K. M., Taylor, M. A. and Herrmann, L. R., "Numerical Biaxial Characterization for Concrete," J. Engr. Mech. Div., ASCE, V. 100, n. EM5, Oct. 1974, p. 935-948.

27. Saenz, L. P., Disc. of "Equation for the Stress-Strain Curve of Concrete," by Disayi and Krishnan, J. ACI, Proc. V. 61, n. 9, Sept. 1964.

28. Shah, S. P. and Winter, G., "Inelastic Behavior and Fracture of Concrete," J. ACI, Proc. V. 63, n. 9, Sept. 1966, p. 925-980.

29. Shah, S. P. and McGarry, F. J., "Griffith Fracture Criterion and Concrete," J. Engr. Mech. Div., ASCE, V. 97, n. EM6, Dec. 1971.

30. Shah, S. P., and Chandra, S., "Critical Stress, Volume Change and Microcracking of Concrete," J. ACI, Proc. V. 65, n. 9, Sept. 1968.

31. Shah, S. P. and Chandra, S., "Concrete Subjected to Cyclic and Sustained Loading," J. ACI, Proc. V. 67, n. 10, Oct. 1970, p. 816-825.

32. Slate, F. O. and Matheus, R. E., "Volume Changes on Setting and Curing of Cement Paste and Concrete from Zero to Seven Days," J. ACI, Proc. V. 64, n. 1, Jan. 1967, p. 34-39.

33. Taylor, M. A. and Broms, B. B., "Shear-Bond Strength Between Coarse Aggregate and Cement Paste or Mortar," J. ACI, Proc. V. 61, n. 8, Aug. 1964, p. 939-958.

34. Taylor, M. A., "General Behavior Theory for Cement Pastes, Mortars, and Concretes," J. ACI, Proc. V. 68, n. 10, Oct. 1971, p. 756-762.

35. Wu, Han-Chin, "Dual Failure Criterion for Plain Concrete," J. Engr. Mech. Div., ASCE, V. 100, n. EM6, Dec. 1974, p. 1167-1181.

APPENDIX A

CONSTITUTIVE RELATIONS FOR AN ORTHOTROPIC MATERIAL

For an incrementally linear, orthotropic material, the constitutive properties are defined along the material axes. For material coordinates, 1-2, the relation between the change in stress and the change in strain, is given by

$$\begin{bmatrix} d\sigma_1 \\ d\sigma_2 \\ d\tau_{12} \end{bmatrix} = \frac{1}{1-\nu_{12}\nu_{21}} \begin{bmatrix} E_1 & \nu_{21}E_1 & 0 \\ \nu_{12}E_2 & E_2 & 0 \\ 0 & 0 & (1-\nu_{12}\nu_{21})G_{12} \end{bmatrix} \begin{bmatrix} d\varepsilon_1 \\ d\varepsilon_2 \\ d\nu_{12} \end{bmatrix} \qquad (A.1)$$

where

(for i = 1,2

and j = 1,2)

E_i = modulus of elasticity along the ith direction,

G_{12} = shear-modulus

and ν_{ij} characterizes strain in the jth direction produced by stress in the ith direction.

The constitutive matrix is symmetric (from energy considerations) therefore,

$$E_1\nu_{21} = E_2\nu_{12} \qquad (A.2)$$

Introducing an "equivalent" Poisson's ratio, ν, such that

$$\nu^2 = \nu_{12}\nu_{21} \qquad (A.3)$$

the following is obtained

$$\nu_{12} = \nu\sqrt{E_1/E_2}$$
$$\nu_{21} = \nu\sqrt{E_2/E_1} \qquad (A.4)$$

Substituting in Eq. A.1, the constitutive relation becomes

$$\begin{bmatrix} d\sigma_1 \\ d\sigma_2 \\ d\tau_{12} \end{bmatrix} = \frac{1}{1-\nu^2} \begin{bmatrix} E_1 & \nu\sqrt{E_1 E_2} & 0 \\ & E_2 & 0 \\ \text{SYM} & & (1-\nu^2)G_{12} \end{bmatrix} \begin{bmatrix} d\varepsilon_1 \\ d\varepsilon_2 \\ d\nu_{12} \end{bmatrix} \qquad (A.5.a)$$

or more simply,

$$\{d\sigma\} = [D]\ \{d\varepsilon\} \qquad (A.5.b)$$

where [D] = constitutive (or elasticity) matrix in the material coordinates.

Let the material coordinate system be at an angle, θ, with the global coordinate system; then the constitutive matrix, [D'], in the global coordinates, is given by

$$[D'] = [T]^T\ [D]\ [T] \qquad (A.6)$$

where [T] = the transformation matrix for strains, so that

$$\{d\varepsilon\} = [T]\ \{d\varepsilon'\} \qquad (A.7)$$

with $\{d\varepsilon'\}$, indicating the changes in strains in the global coordinates, corresponding to the local changes, $\{d\varepsilon\}$.

$$[T] = \begin{bmatrix} \cos^2\theta & \sin^2\theta & \cos\theta\sin\theta \\ \sin^2\theta & \cos^2\theta & -\cos\theta\sin\theta \\ -2\cos\theta\sin\theta & 2\cos\theta\sin\theta & \cos^2\theta-\sin^2\theta \end{bmatrix} \qquad (A.8)$$

Substituting the value of, [D] from Eq. A.5 and, [T]from Eq. A.8, in

Eq. A.6, we get

$$D'(1,1) = [\cos^2\theta(E_1\cos^2\theta+\nu\sqrt{E_1E_2}\sin^2\theta) + \sin^2\theta(\nu\sqrt{E_1E_2}\cos^2\theta + E_2\sin^2\theta) + 4\cos^2\theta\sin^2\theta(1-\nu^2)G]\frac{1}{1-\nu^2}$$

$$D'(1,2) = [\cos^2\theta(E_1\sin^2\theta+\nu\sqrt{E_1E_2}\cos^2\theta) + \sin^2\theta(\nu\sqrt{E_1E_2}\sin^2\theta + E_2\cos^2\theta) - 4\cos^2\theta\sin^2\theta(1-\nu^2)G]\frac{1}{1-\nu^2}$$

$$D'(2,1) = D'(1,2)$$

$$D'(2,2) = [\sin^2\theta(E_1\sin^2\theta+\nu\sqrt{E_1E_2}\cos^2\theta) + \cos^2\theta(\nu\sqrt{E_1E_2}\sin^2\theta + E_2\cos^2\theta) + 4\cos^2\theta\sin^2\theta(1-\nu^2)G]\frac{1}{1-\nu^2}$$

$$D'(1,3) = \cos\theta\sin\theta[\cos^2\theta(E_1-\nu\sqrt{E_1E_2}) + \sin^2\theta(\nu\sqrt{E_1E_2}-E_2) -2(1-\nu^2)(\cos^2\theta-\sin^2\theta)G]\frac{1}{1-\nu^2}$$

$$D'(3,1) = D'(1,3)$$

$$D'(2,3) = \cos\theta\sin\theta[\sin^2\theta(E_1-\nu\sqrt{E_1E_2}) + \cos^2\theta(\nu\sqrt{E_1E_2}-E_2) + 2(1-\nu^2)(\cos^2\theta-\sin^2\theta)G]\frac{1}{1-\nu^2}$$

$$D'(3,2) = D'(2,3)$$

$$D'(3,3) = \cos^2\theta\sin^2\theta\,(E_1+E_2-2\nu\sqrt{E_1E_2})\frac{1}{1-\nu^2} + (\cos^2\theta-\sin^2\theta)^2 \times (1-\nu^2)G$$

For a value of shear modulus independent of orientation let,

$$(1-\nu^2)G = (1-\nu^2)D'(3,3) = \frac{1}{4}\,(E_1+E_2-2\nu\sqrt{E_1E_2}) \tag{A.9}$$

Substitute Eq. A.9 into the expressions for [D']:

$$[D'] = \frac{1}{1-\nu^2}\begin{bmatrix} E_1\cos^2\theta+E_2\sin^2\theta & \nu\sqrt{E_1E_2} & \frac{1}{2}(E_1-E_2)\sin\theta\cos\theta \\ & E_1\sin^2\theta+E_2\cos^2\theta & \frac{1}{2}(E_1-E_2)\sin\theta\cos\theta \\ \text{SYM} & & \frac{1}{4}(E_1+E_2-2\nu\sqrt{E_1E_2}) \end{bmatrix} \tag{A.10}$$

In Eq. A.10 the terms containing Poisson's ratio, ν, as well as the shear modulus are independent of orientation.

Relation between change in stress, $\{d\sigma'\}$, and change in strain, $\{d\varepsilon'\}$, in global coordinates is, therefore,

$$\{d\sigma'\} = [D']\,\{d\varepsilon'\} \tag{A.11}$$

or in the material coordinates:

$$\begin{bmatrix} d\sigma_1 \\ d\sigma_2 \\ d\sigma_{12} \end{bmatrix} = \frac{1}{1-\nu^2}\begin{bmatrix} E_1 & \nu\sqrt{E_2E_2} & 0 \\ & E_2 & 0 \\ \text{SYM} & & \frac{1}{4}(E_1+E_2-2\nu\sqrt{E_1E_2}) \end{bmatrix}\begin{bmatrix} d\varepsilon_1 \\ d\varepsilon_2 \\ d\varepsilon_{12} \end{bmatrix} \tag{A.12}$$

APPENDIX B

PROPERTIES OF THE FINITE ELEMENT

B.1 INTRODUCTION The finite element used in this study is a four-noded, quadrilateral, isoparametric element with two translational degrees of freedom at each node. It is formulated using an intrinsic coordinate system, which is defined by element geometry. The element coordinates ξ and η are non-dimensional, with a range $\xi = -1$, $\xi = +1$, $\eta = -1$, and $\eta = +1$. The element satisfies the "patch test" (5).

B.2 FORMULATION Let us consider a quadrilateral element having eight degrees of freedom, u_i and v_i at each of four nodes, i. The element has straight sides but is otherwise of arbitrary shape and may be considered a distortion of a "parent" rectangular element (Fig. B.1). The coordinate (X,Y) of any point in the element may be expressed as follows:

$$X = \sum_{i=1}^{4} N_i X_i \qquad \text{(B.1.a)}$$

$$Y = \sum_{i=1}^{4} N_i Y_i \qquad \text{(B.1.b)}$$

where N_i is the shape function and X_i and Y_i are the x and y coordinates of node, i.

The shape functions are obtained as follows:

$$X = a_1+a_2\xi+a_3\eta+a_4\xi\eta \qquad \text{(B.2.a)}$$

$$Y = b_1+b_2\xi+b_3\eta+b_4\xi\eta \qquad \text{(B.2.b)}$$

substituting $x = x_1$ at $\xi = \eta = -1$, etc. in Eq. B.2.a, four simultaneous

equations are obtained in terms of nodal coordinates. Replacing a's by nodal coordinates,

$$N_i = (1+\xi\xi_i)\ (1+\eta\eta_i)/4 \tag{B.3}$$

where ξ_i and η_i are the local coordinates of node, i.

Displacements within the element are defined by the same interpolation functions as used to define the element shape:

$$u = \sum_{i=1}^{4} N_i u_i \tag{B.4.a}$$

$$v = \sum_{i=1}^{4} N_i v_i \tag{B.4.b}$$

Where u_i and v_i are the x- and y-displacements of the node, i. It should be noted that u and v are parallel and perpendicular to the global coordinates.

B.3 STRAIN AT A POINT The strains at a point may be obtained by taking appropriate derivatives of displacements.

Strains are obtained from Eqs. B.4 as follows:

$$\varepsilon_x = \frac{\partial u}{\partial x} = \sum_{i=1}^{4} N_{i,x}\, u_i \tag{B.5.a}$$

$$\varepsilon_y = \frac{\partial v}{\partial y} = \sum_{i=1}^{4} N_{i,y}\, v_i \tag{B.5.b}$$

$$\gamma_{xy} = \frac{\partial u}{\partial y} + \frac{\partial v}{\partial x} = \sum_{i=1}^{4} N_{i,y}\, u_i + \sum_{i=1}^{4} N_{i,x}\, v_i \tag{B.5.c}$$

where commas denote partial differentiation.

Relations between derivatives in the two coordinate systems are established by the chain rule of differentiation:

$$N_{i,\xi} = N_{i,x}\, X_{,\xi} + N_{i,y}\, Y_{,\xi}$$

$$N_{i,\eta} = N_{i,x}\, X_{,\eta} + N_{i,y}\, Y_{,\eta} \qquad \text{(B.6.a)}$$

$$N_{i,x} = N_{i,\xi}\, \xi_{,x} + N_{i,\eta}\, \eta_{,x}$$

$$N_{i,y} = N_{i,\xi}\, \xi_{,y} + N_{i,\eta}\, \eta_{,y} \qquad \text{(B.6.b)}$$

where i = 1,4

Using Eq. B.6.a the following relations are obtained

$$[J] = \begin{bmatrix} X_{,\xi} & Y_{,\xi} \\ X_{,\eta} & Y_{,\eta} \end{bmatrix} \qquad \text{(B.7)}$$

and

$$[J]^{-1} = \frac{1}{|J|} \begin{bmatrix} Y_{,\eta} & -Y_{,\xi} \\ -X_{,\eta} & X_{,\xi} \end{bmatrix} \qquad \text{(B.8)}$$

where [J] = the Jacobian Matrix and $|J|$ = the Jacobian Determinant

$$= X_{,\xi}\, Y_{,\eta} - X_{,\eta}\, Y_{,\xi}$$

From Eq. B.6.b.,

$$[J]^{-1} = \begin{bmatrix} \xi_{,x} & \eta_{,x} \\ \xi_{,y} & \eta_{,y} \end{bmatrix} \qquad \text{(B.9)}$$

Equating Eqs. B.8 and B.9,

$$\begin{bmatrix} \xi,_x & \eta,_x \\ \xi,_y & \eta,_y \end{bmatrix} = \frac{1}{|J|} \begin{bmatrix} Y,_\eta & -Y,_\xi \\ X,_\eta & X,_\xi \end{bmatrix} \tag{B.10}$$

From Eqs. B.1, we get

$$\begin{aligned} X,_\xi &= \Sigma\, N_i,_\xi\, X_i \\ X,_\eta &= \Sigma\, N_i,_\eta\, X_i \\ X,_\xi &= \Sigma\, N_i,_\xi\, Y_i \\ Y,_\eta &= \Sigma\, N_i,_\eta\, Y_i \end{aligned} \qquad (i = 1,4) \tag{B.11}$$

The strain displacement relation $\{\varepsilon\} = [B]\{u\}$ may be written in matrix form:

$$\begin{bmatrix} \varepsilon_x \\ \varepsilon_y \\ \varepsilon_{xy} \end{bmatrix} = \frac{1}{|J|} \left[\begin{array}{cc|cc|cc|cc} \alpha_1 & 0 & \alpha_2 & 0 & \alpha_3 & 0 & \alpha_4 & 0 \\ 0 & \beta_1 & 0 & \beta_2 & 0 & \beta_3 & 0 & \beta_4 \\ \beta_1 & \alpha_1 & \beta_2 & \alpha_2 & \beta_3 & \alpha_3 & \beta_4 & \alpha_4 \end{array}\right] \begin{bmatrix} u_1 \\ v_1 \\ u_2 \\ v_2 \\ u_3 \\ v_3 \\ u_4 \\ v_4 \end{bmatrix} \tag{B.12}$$

where $\alpha_i = N_i,_x\, |J|$

$$\beta_i = N_i,_y\, |J| \qquad (i = 1,4)$$

In symbolic terms, Eq. B.12 may be written as

$$\varepsilon = Bu = \frac{\bar{B}}{|J|}\, u \tag{B.13}$$

B.4 ELEMENT STIFFNESS MATRIX

The element stiffness matrix is given by

$$K = \int_{Vol} B^T D B \; dVol = \int_{area} t \; B^T D B \; dArea \qquad (B.14)$$

where

B = strain displacement relationship matrix

D = elasticity matrix

t = the element thickness

Integration is done over the area of the element.

Eq. B.14 may be rewritten for the purpose of numerical integration

$$K = \int_{-1}^{1} \int_{-1}^{1} t \; B^T D B \; |J| \; d\xi \; d\eta \qquad (B.15.a)$$

or

$$K = \int_{-1}^{1} \int_{-1}^{1} t \; \bar{B}^T D \bar{B} \; \frac{d\xi d\eta}{|J|} \qquad (B.15.b)$$

Numerical integration uses Gauss quadrature (5) which locates the integration points to achieve best accuracy for a given number of sampling points. Sampling points are located symmetrically with respect to the center of the interval. In two dimensions we obtain the following summation,

$$K = \sum_j \sum_k H_j \; H_k \; t_{jk} \; \bar{B}^T_{jk} \; D_{jk} \; \bar{B}_{jk} \; \frac{1}{|J|_{jk}} \qquad (B.16)$$

where t_{jk}, $\bar{B}_{jk}$, D_{jk} and $|J|_{jk}$ take on the appropriate values at each integration point (ξ_j, η_k). H_j and H_k are the appropriate weighting factors.

B.4 ELEMENT RESIDUAL LOADS

The residual loads due to inelastic behavior for the element are given by

$$\delta R = \int_{area} t\, B^T\, \delta\sigma_r\, dA \tag{B.17}$$

where the residual stresses, $\delta\sigma_r$, are given by:

$$\delta\sigma_r = \begin{bmatrix} \delta\sigma_{xr} \\ \delta\sigma_{yr} \\ \delta\sigma_{xyr} \end{bmatrix} \tag{B.18}$$

In terms of the non-dimensional coordinates, Eq. B.17 may be re-written

$$\delta R = \int_{-1}^{1} \int_{-1}^{1} t\, B^T \delta\sigma_r\, d\xi\, d\eta \tag{B.19}$$

Numerical integration, to obtain the residual loads takes the following form

$$\delta R = \sum_j \sum_k H_j\, H_k\, t_{jk}\, \bar{B}^T_{jk}\, \delta\sigma_{rjk} \tag{B.20}$$

where H_j, H_k, t_{jk} and $\bar{B}_{jk}$ are defined in Eq. B.16.

TABLE 4.1

STRESSES AND STRAINS IN CONCRETE AT DIFFERENT STAGES OF CRACKING FOR NORMAL STRENGTH OF INTERFACE

(Stages of cracking correspond to the cracking maps in Fig. 4.4.)

	d/r = 2/3				d/r = 1/2	
	LINEAR MORTAR		NONLINEAR MORTAR		NONLINEAR MORTAR	
STAGE	STRAIN μin/in	STRESS psi	STRAIN μin/in	STRESS psi	STRAIN μin/in	STRESS psi
1	-400	-1264	-400	-1217	-400	-1258
2	-400	-1260	-400	-1215	-400	-1255
3	-400	-1255	-400	-1209	-400	-1250
4	-450	-1380	-450	-1331	-400	-1222
5	-750	-2296	-800	-2188	-600	-1760
6	-850	-2600	-950	-2493	-850	-2356
7	-900	-2750	-1000	-2581	-850	-2360
8.a	-950	-2890				
8.b			-1100	-2743	-900	-2460
9			-1150	-2760	-950	-2496
10			-1350	-2969	-1200	-2870

TABLE 4.2

STRESSES AND STRAINS IN CONCRETE AT DIFFERENT STAGES OF CRACKING FOR ZERO TENSILE AND COHESIVE STRENGTH OF INTERFACE

(Stages of cracking correspond to the cracking maps in Fig. 4.6.)

	d/r = 2/3			
	LINEAR MORTAR		NONLINEAR MORTAR	
STAGE	STRAIN μin/in	STRESS psi	STRAIN μin/in	STRESS psi
1	-50	-153	-50	-157
2	-900	-2727	-850	-2289
3	-900	-2724	-850	-2287
4.a	-950	-2868		
4.b			-1050	-2577
5			-1350	-2952

TABLE 4.3

STRESSES AND STRAINS IN CONCRETE AT DIFFERENT STAGES OF CRACKING FOR ZERO COHESIVE AND TENSILE STRENGTHS AND ZERO ANGLE OF INTERNAL FRICTION OF INTERFACE

(Stages of cracking correspond to the cracking maps in Fig. 4.9.)

	d/r = 2/3			
	LINEAR MORTAR		NONLINEAR MORTAR	
STAGE	STRAIN μin/in	STRESS psi	STRAIN μin/in	STRESS psi
1	-50	-157	-50	-157
2	-50	-134	-50	-134
3	-200	-532	-200	-521
4	-250	-627	-250	-616
5	-300	-707	-300	-692
6	-400	-944	-400	-910
7	-650	-1541	-650	-1438
8	-650	-1538	-650	-1437
9.a	-750	-1778		
9.b			-850	-1808
10			-1150	-2277
11			-1450	-2604

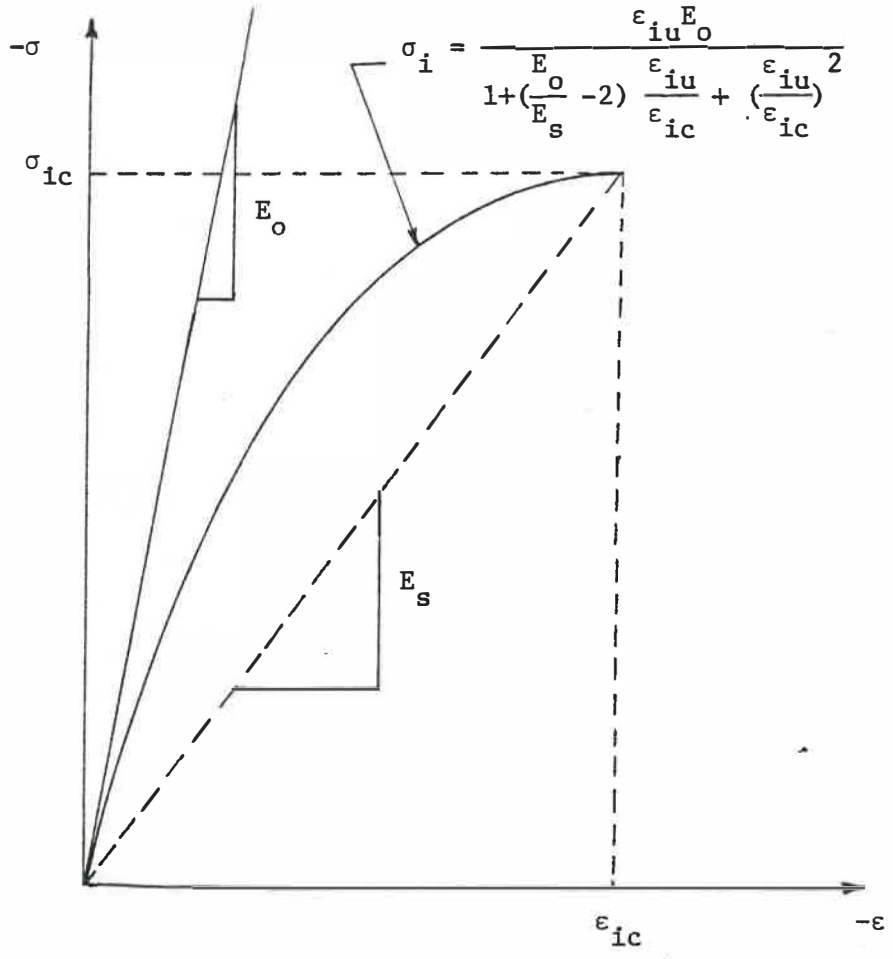

FIGURE 2.1. EQUIVALENT UNIAXIAL STRESS-STRAIN CURVE

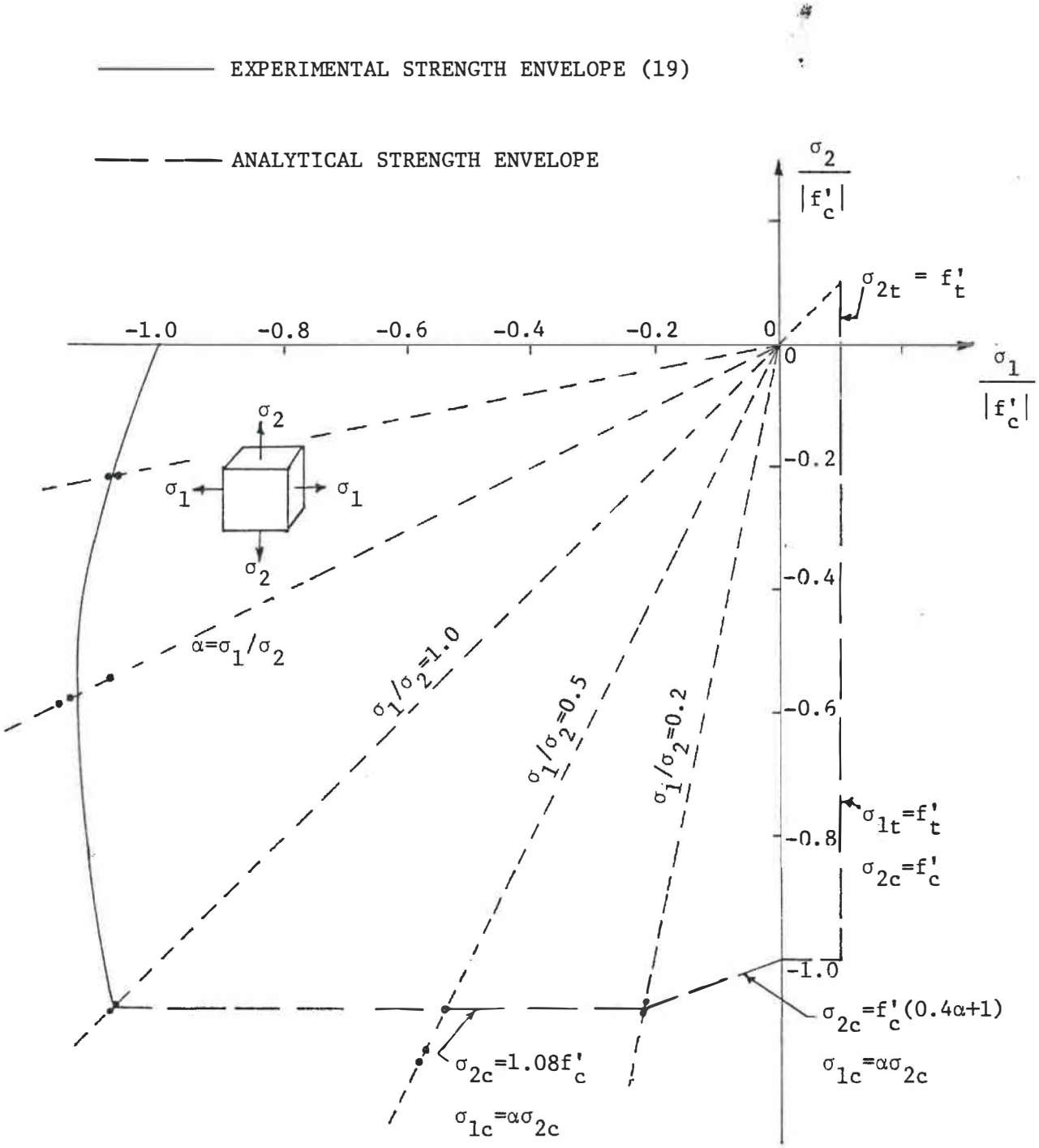

FIGURE 2.2. EXPERIMENTAL AND ANALYTICAL STRENGTH ENVELOPES FOR MORTAR

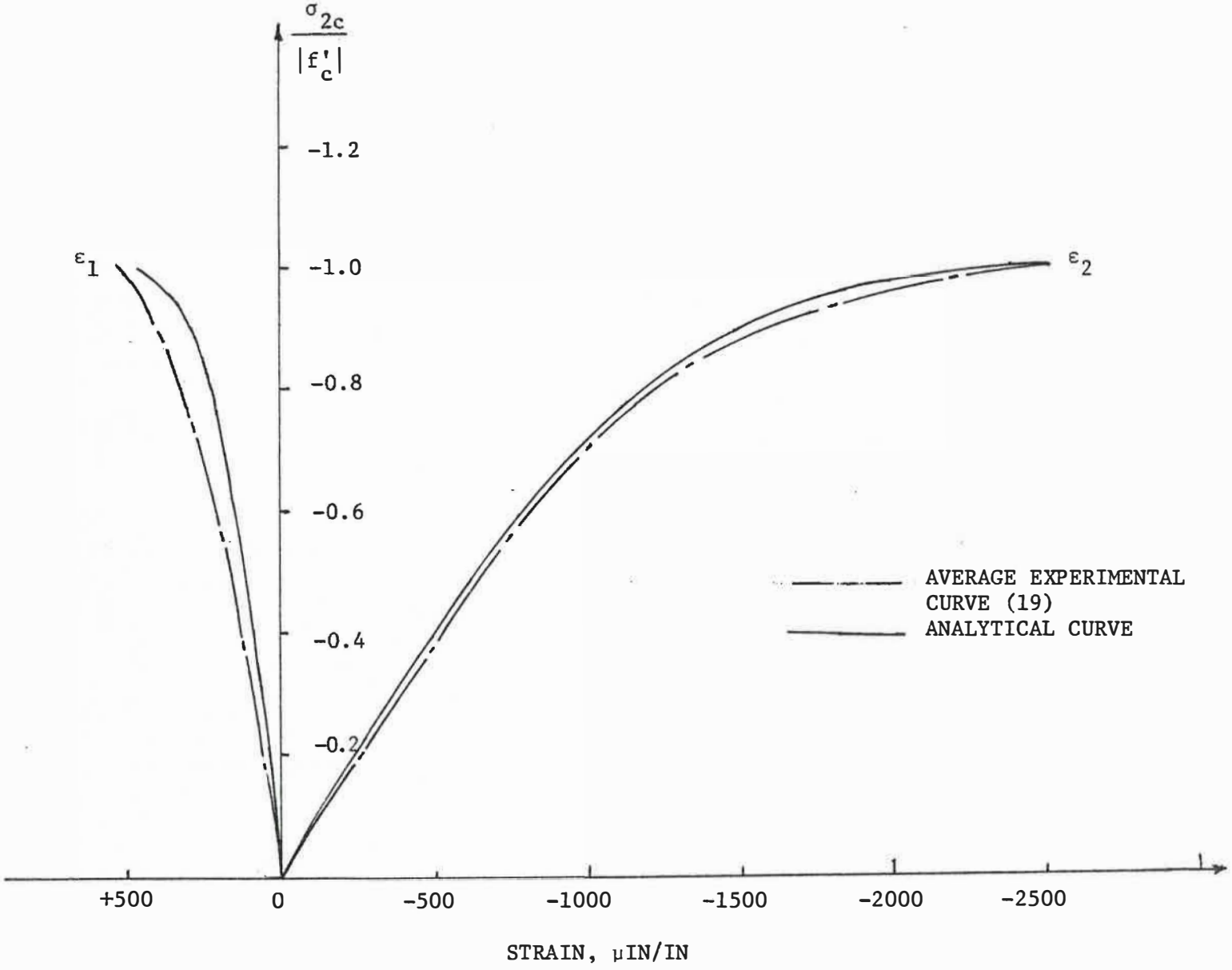

FIGURE 2.3. COMPARISON OF EXPERIMENTAL AND ANALYTICAL UNIAXIAL LOADING CURVES FOR MORTAR

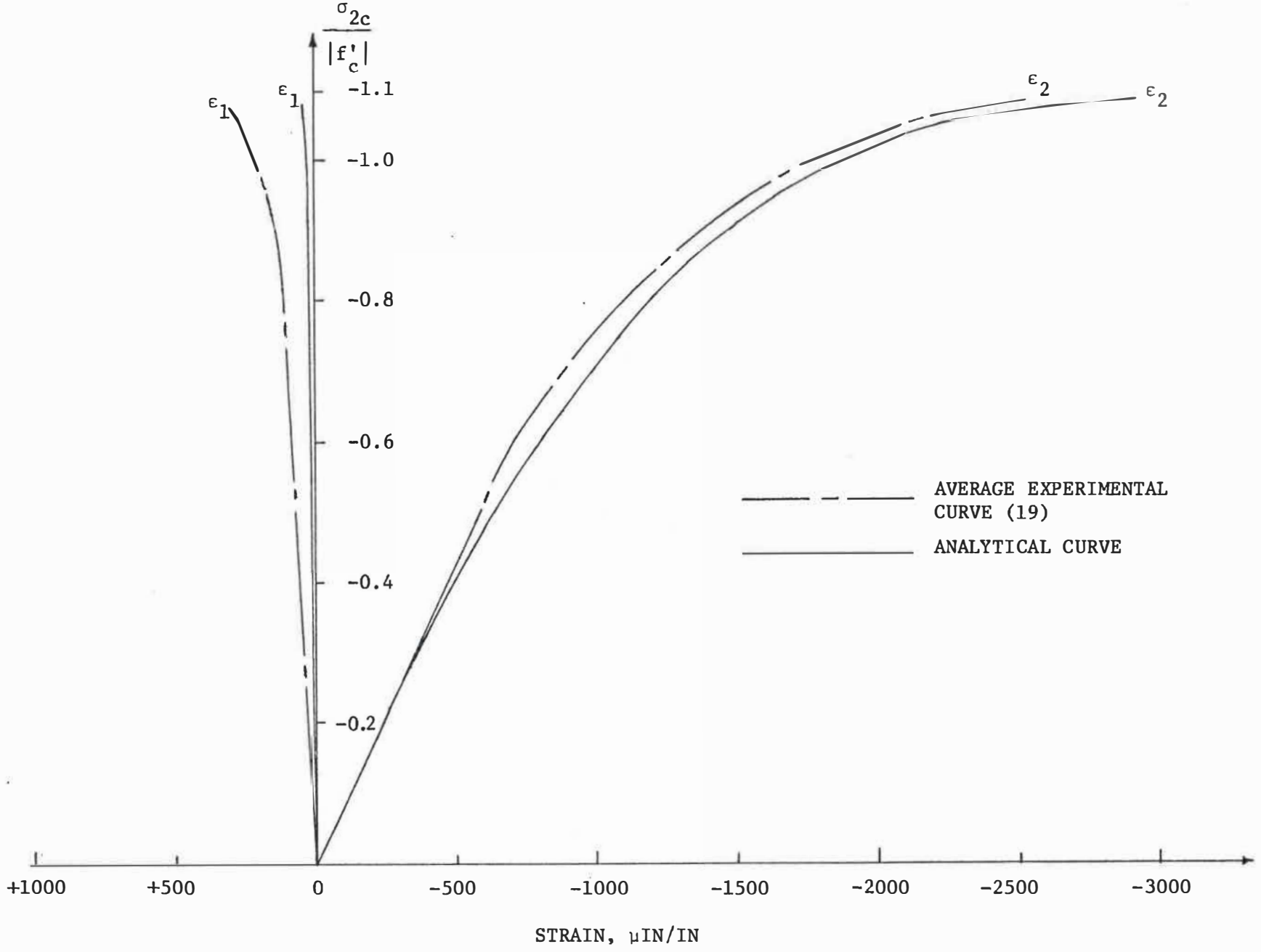

FIGURE 2.4. COMPARISON OF ANALYTICAL AND EXPERIMENTAL BIAXIAL LOADING CURVES FOR MORTAR, α=0.2

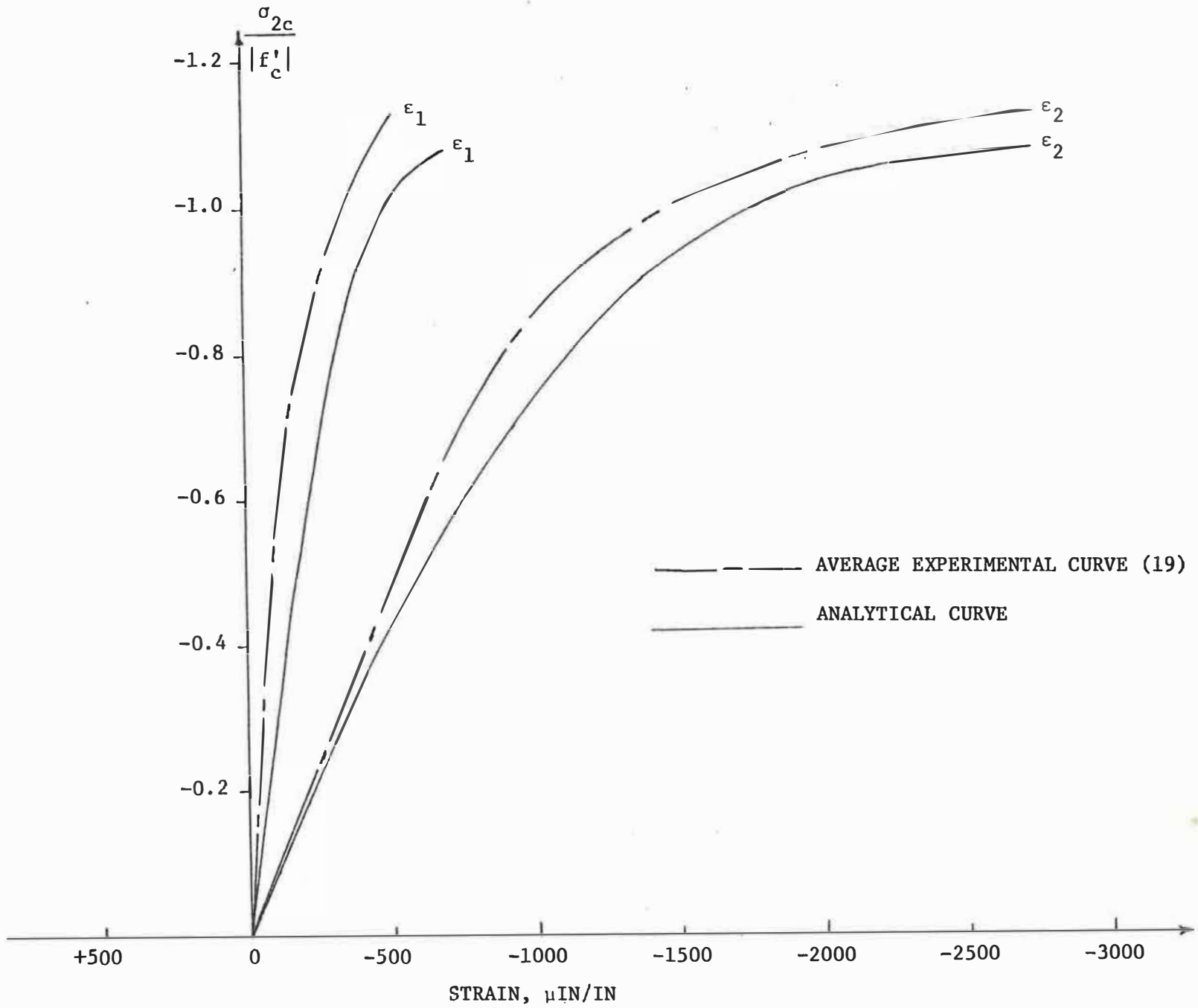

FIGURE 2.5. COMPARISON OF EXPERIMENTAL AND ANALYTICAL BIAXIAL LOADING CURVES FOR MORTAR, $\alpha = 0.5$

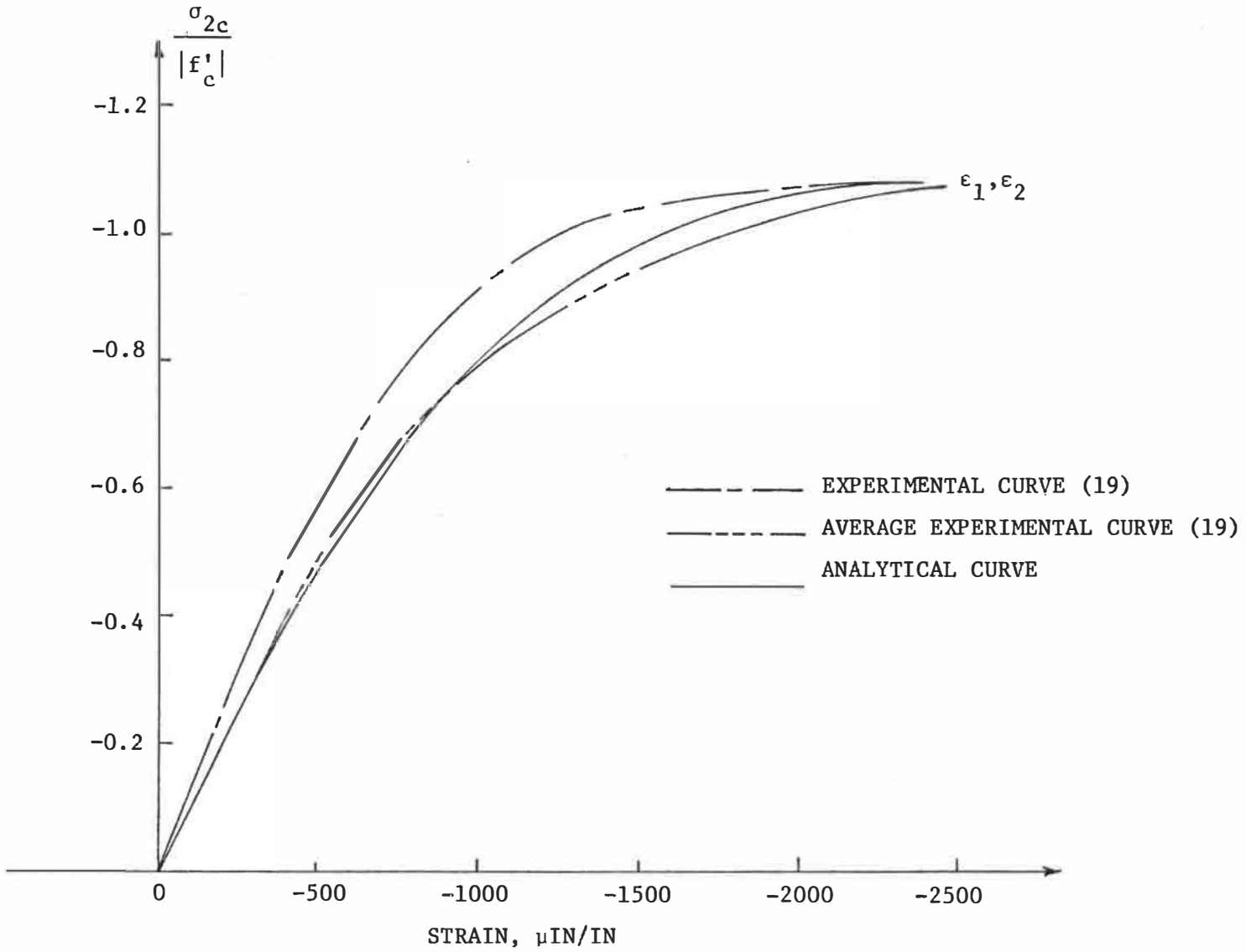

FIGURE 2.6. COMPARISON OF EXPERIMENTAL AND ANALYTICAL BIAXIAL LOADING CURVES FOR MORTAR, α = 1.0

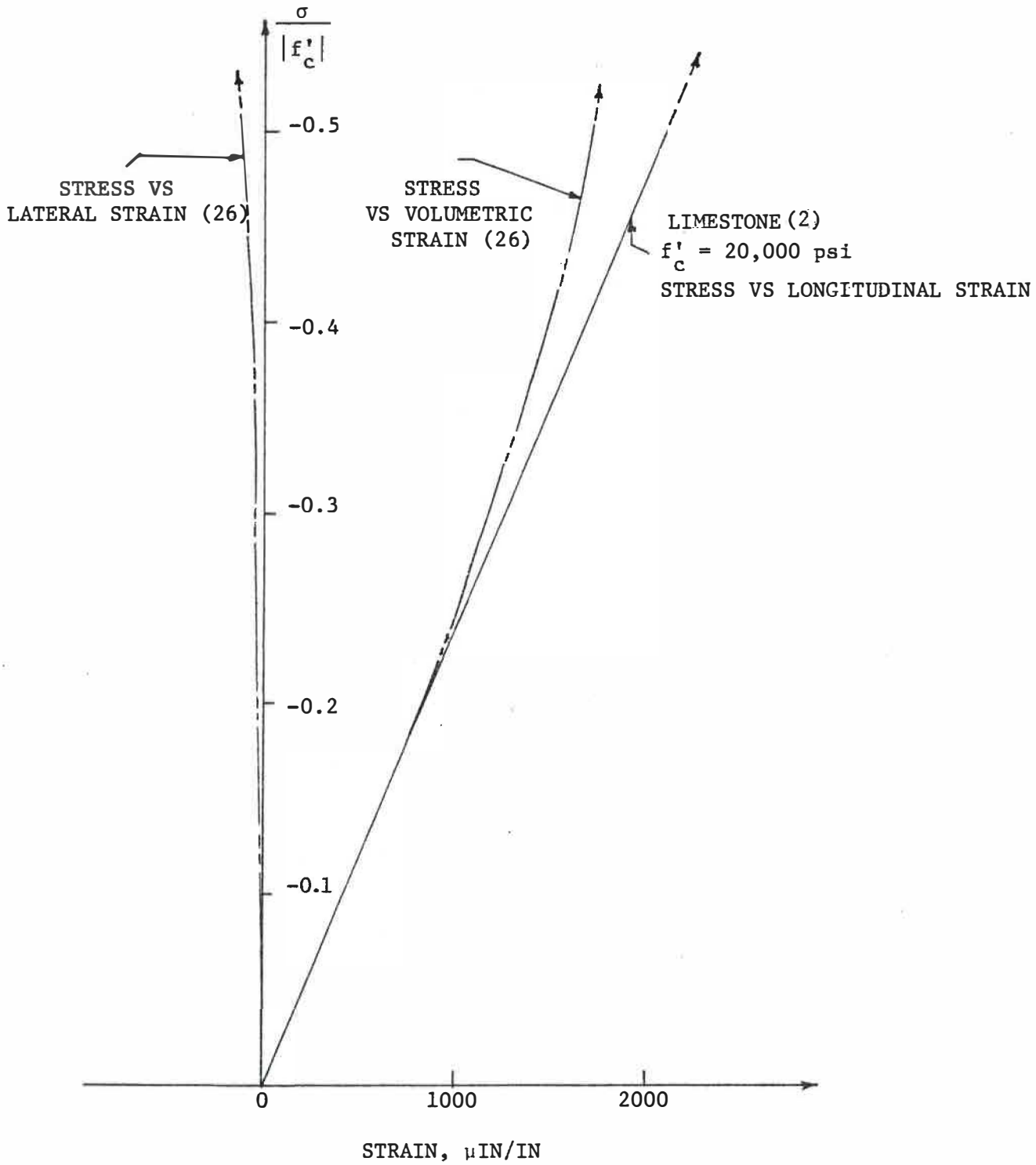

FIGURE 2.7. STRESS STRAIN CURVES FOR STONE

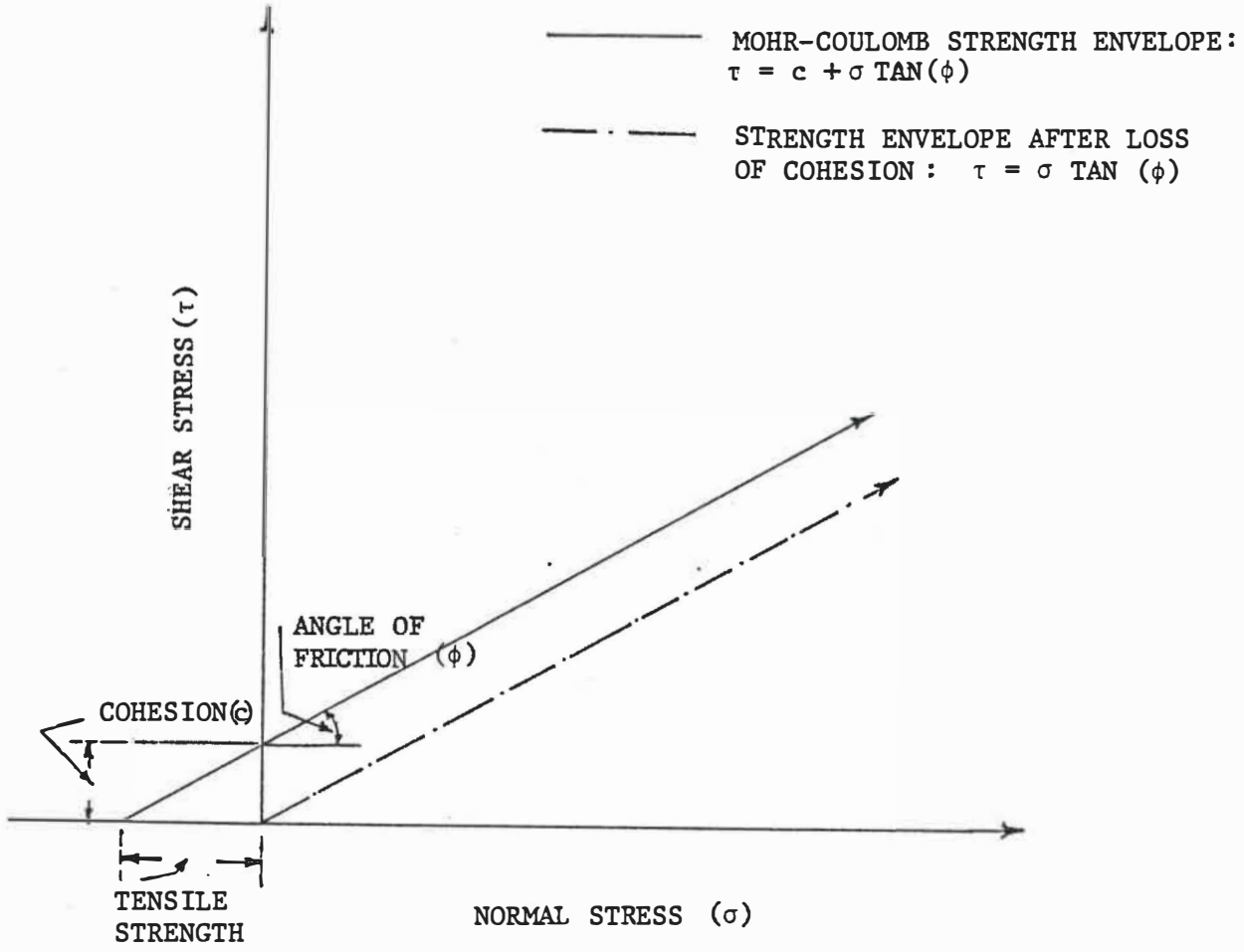

FIGURE 2.8. STRENGTH ENVELOPE FOR INTERFACE

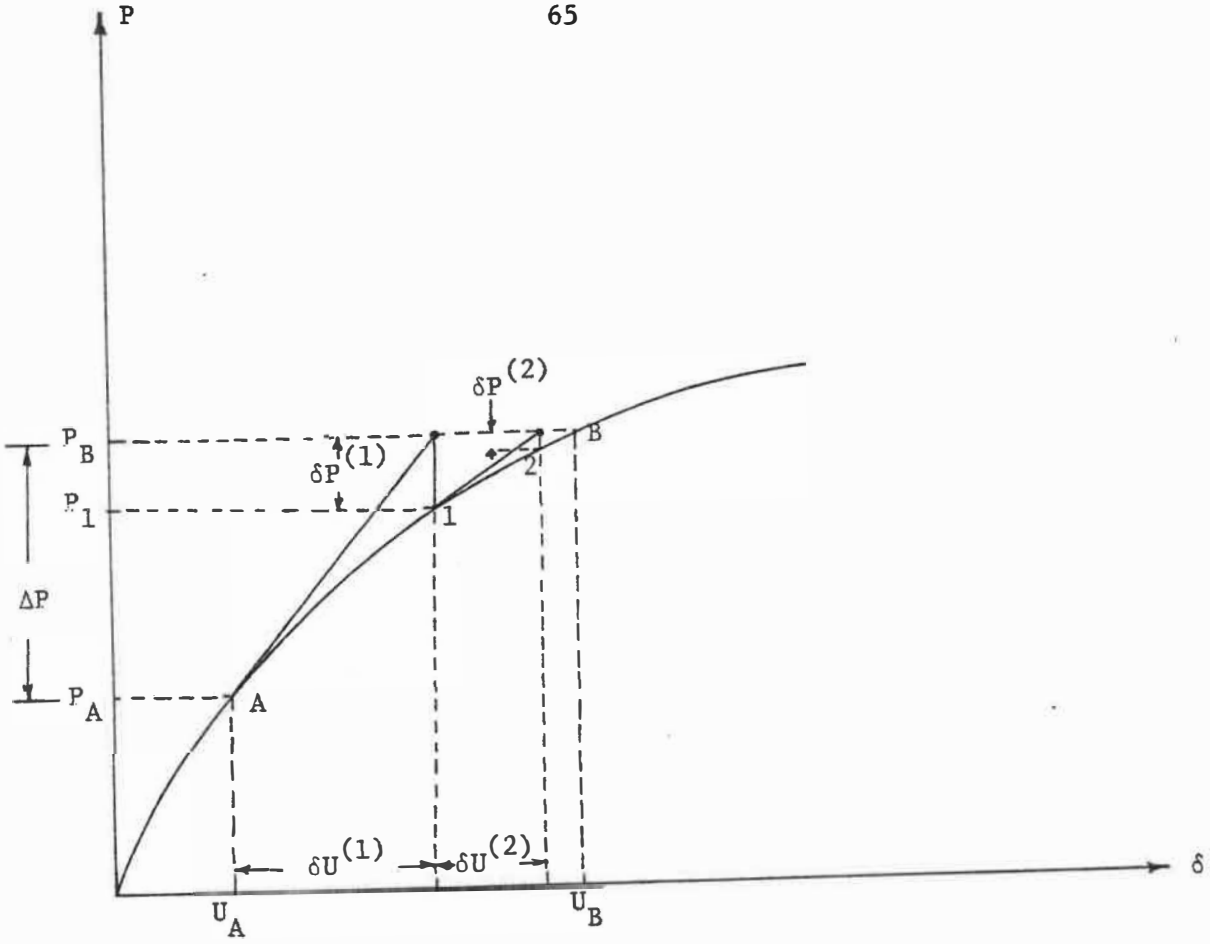

FIGURE 3.1.a. CORRECTION OF LOADS

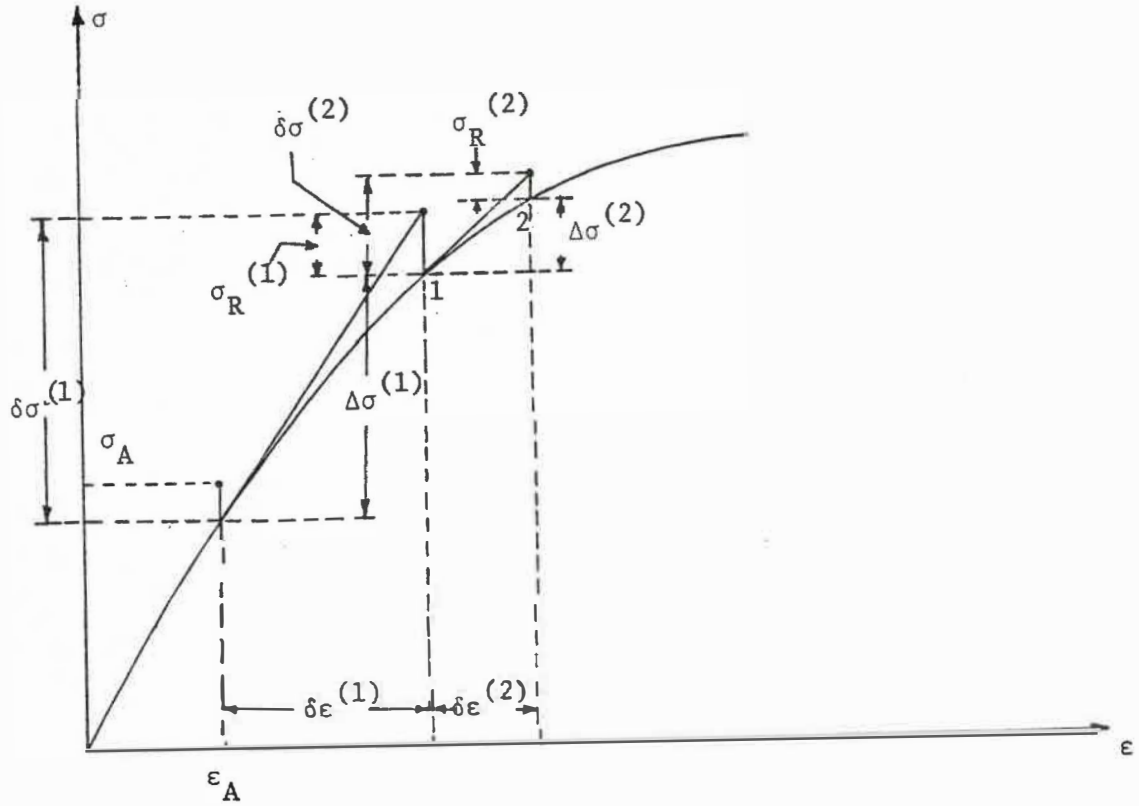

FIGURE 3.1.b. CORRECTION OF STRESSES

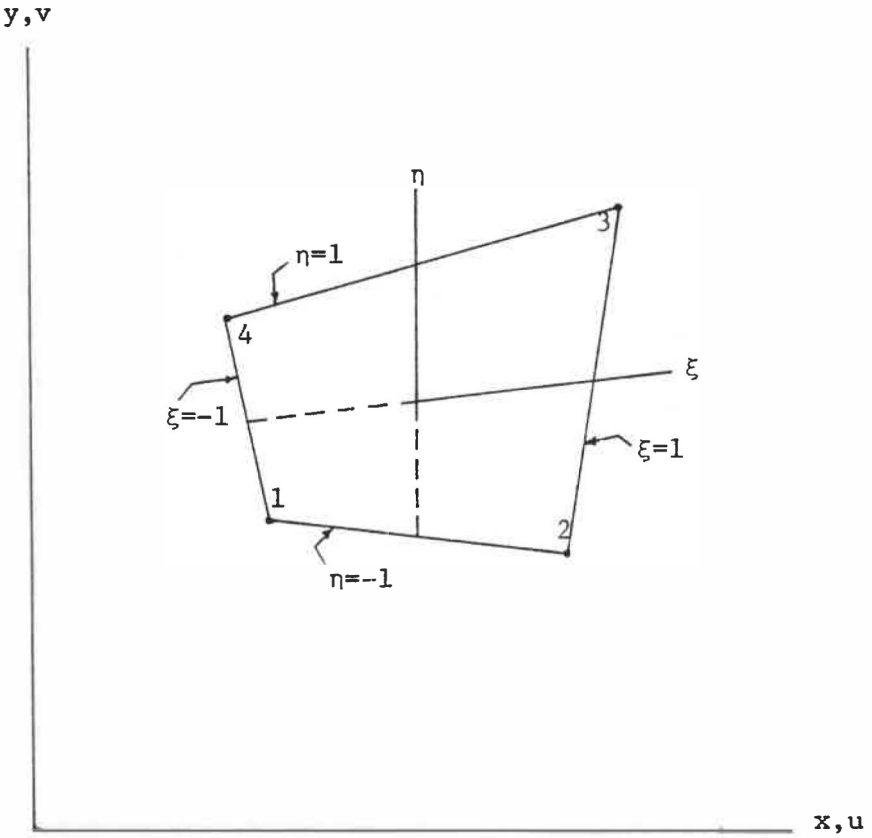

FIGURE B.1.(a). QUADRILATERAL BILINEAR ISOPARAMETRIC ELEMENT

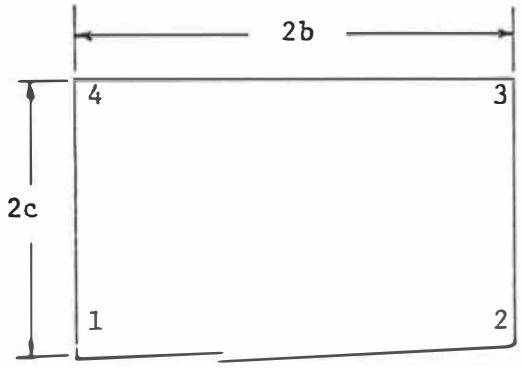

FIGURE B.1.(b) PARENT ELEMENT

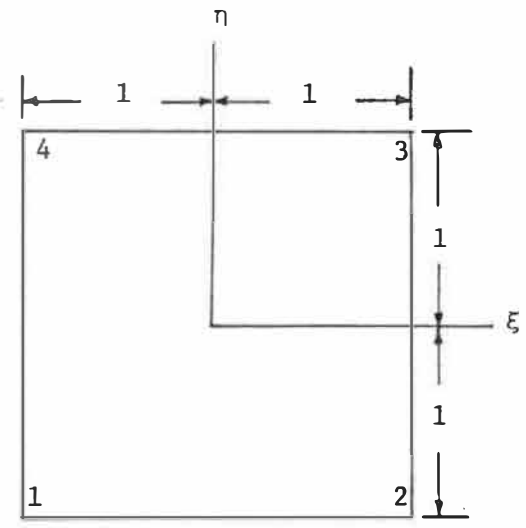

FIGURE B.1.(c). MAPPING INTO SQUARE

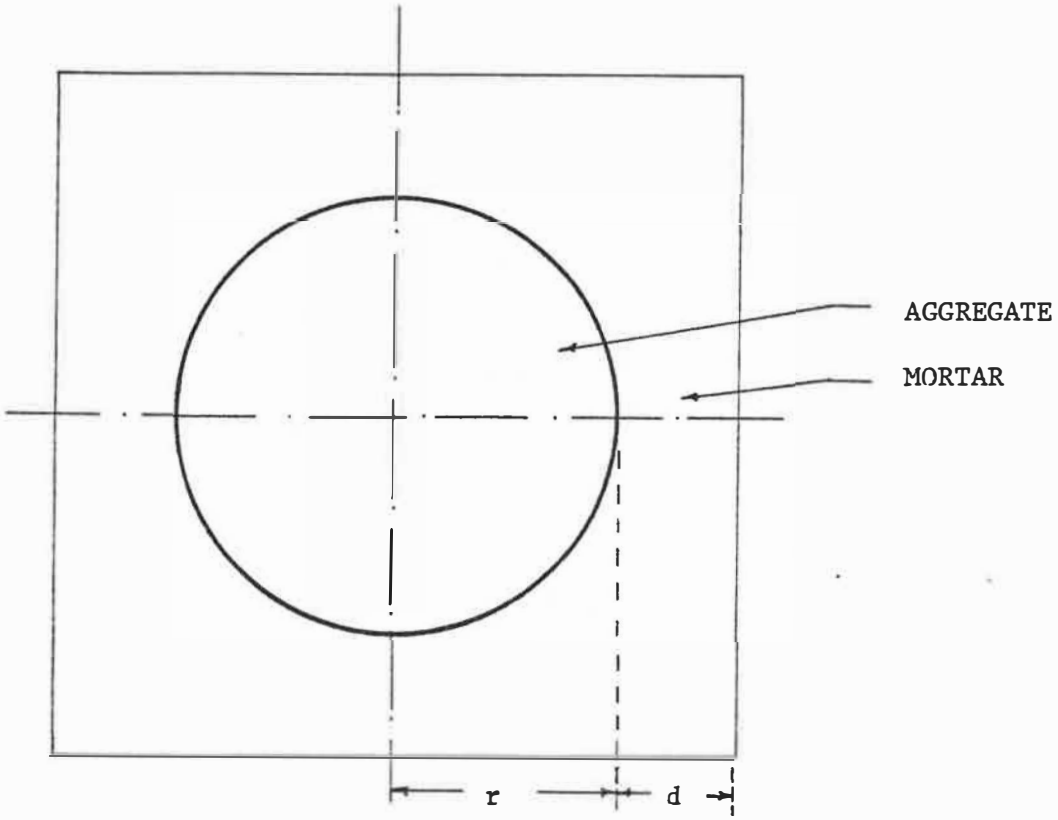

FIGURE 4.1. SHAH AND WINTER'S "STRUCTURAL UNIT" OF CONCRETE

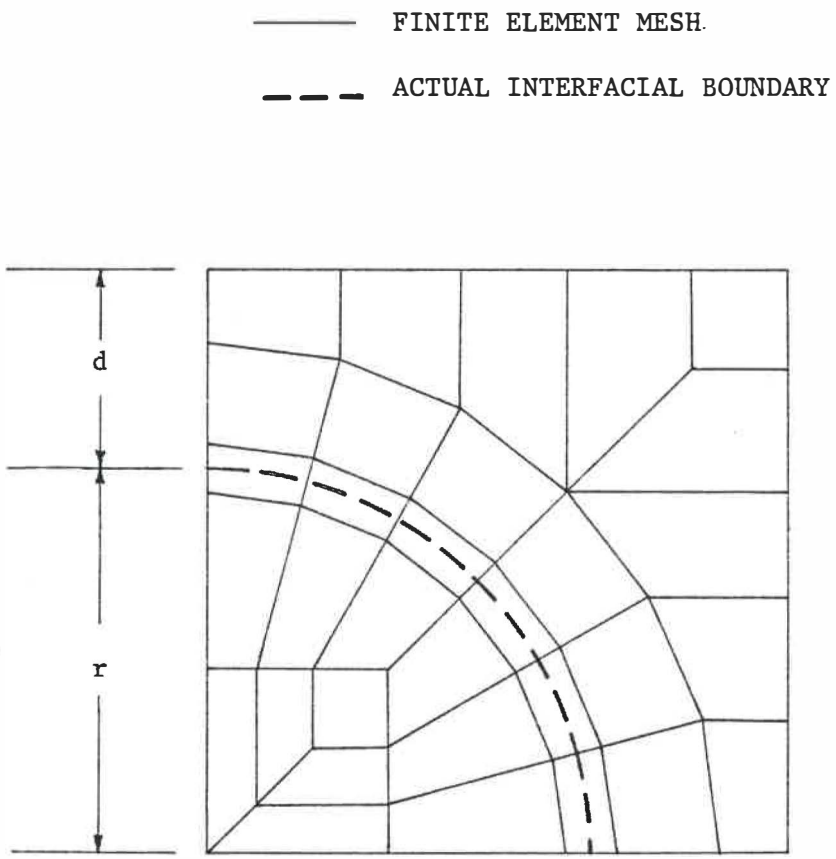

FIGURE 4.2. FINITE ELEMENT MODEL

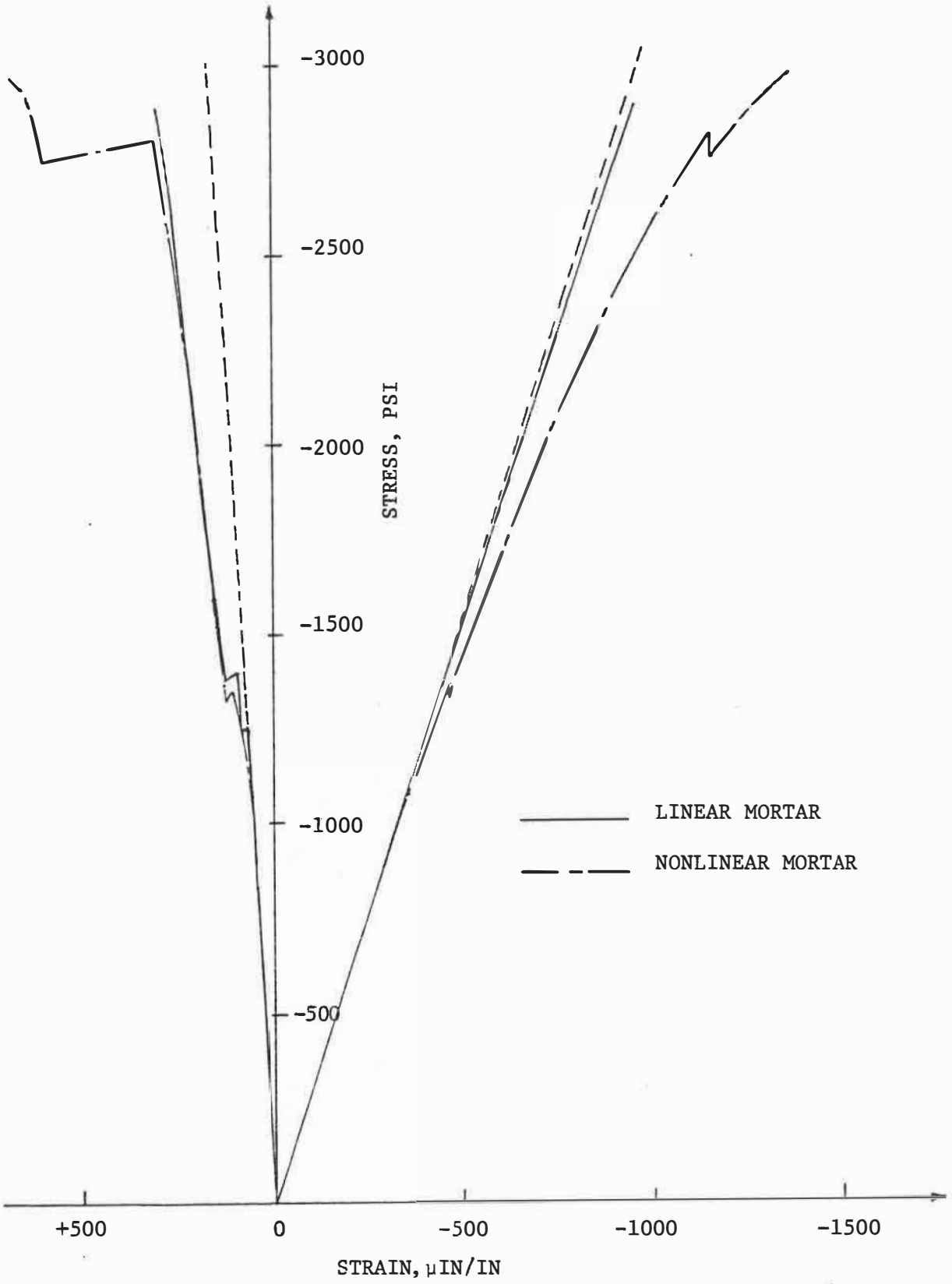

FIGURE 4.3. UNIAXIAL STRESS-STRAIN CURVES FOR CONCRETE WITH NORMAL STRENGTH OF INTERFACE

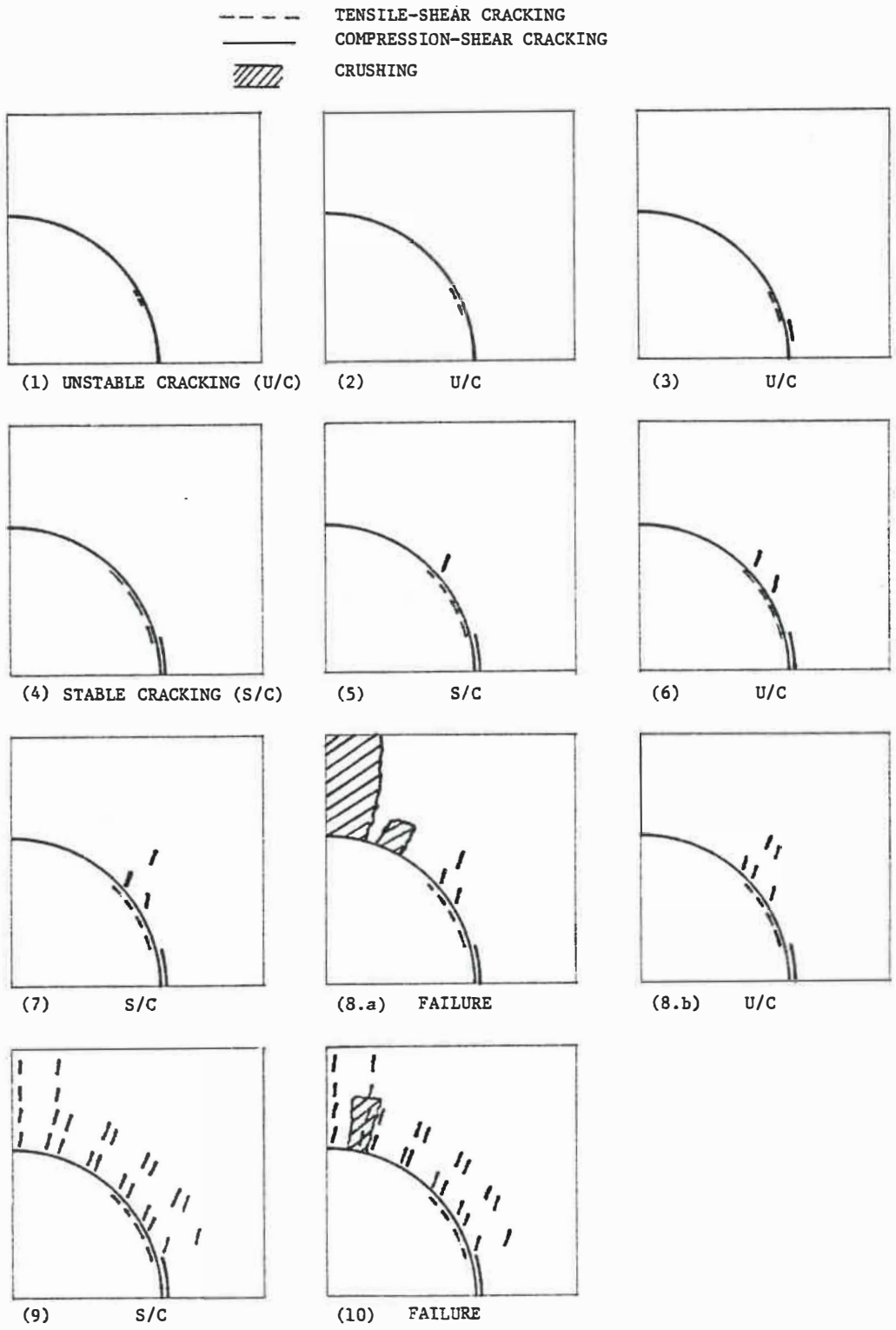

FIGURE 4.4. CRACKING MAPS FOR CONCRETE WITH NORMAL STRENGTH OF INTERFACE (STRAINS AND STRESSES AT DIFFERENT "STAGES" OF CRACKING ARE SHOWN IN TABLE 4.1.)

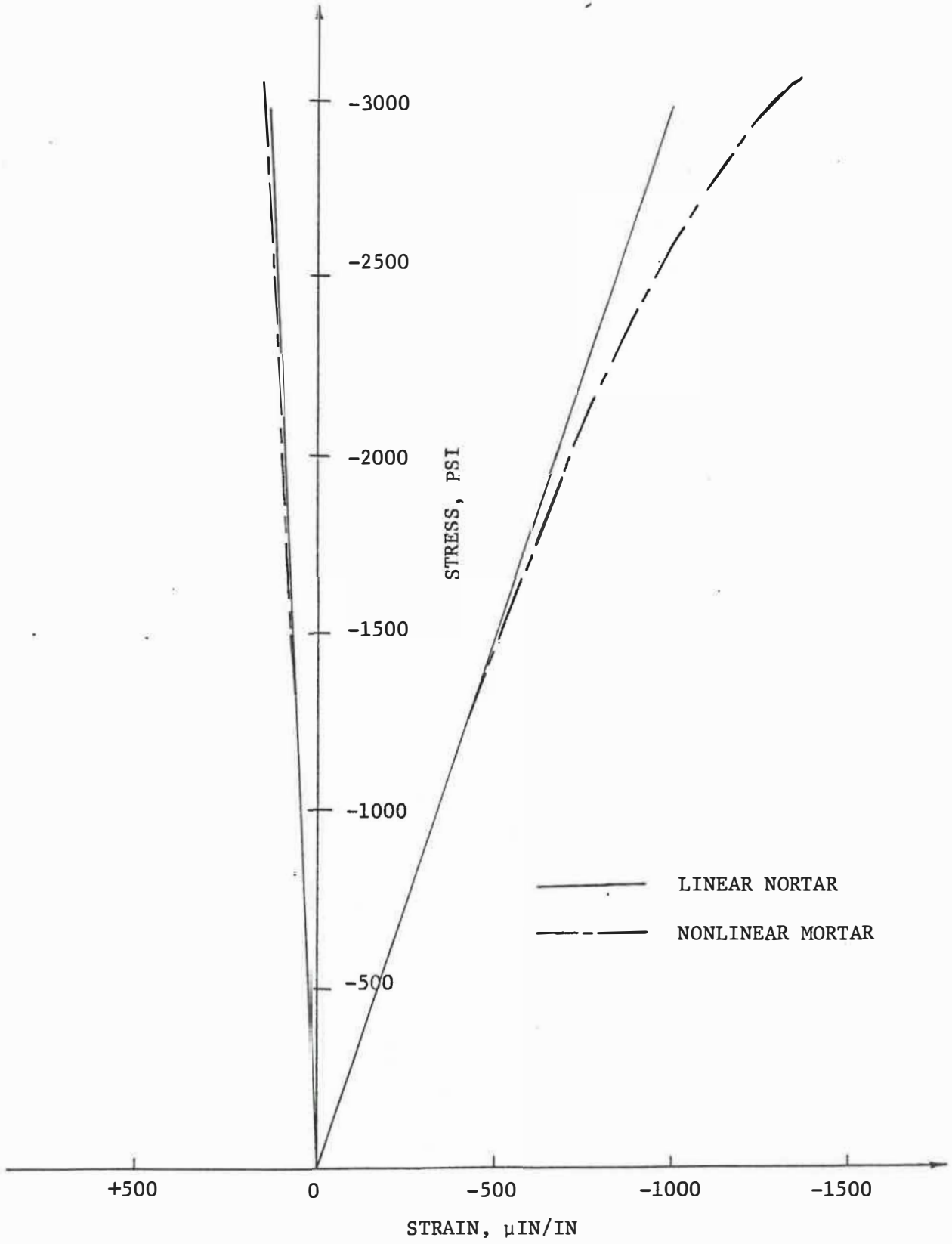

FIGURE 4.5. STRESS-STRAIN CURVE FOR CONCRETE WITH INFINITE INTERFACIAL STRENGTH

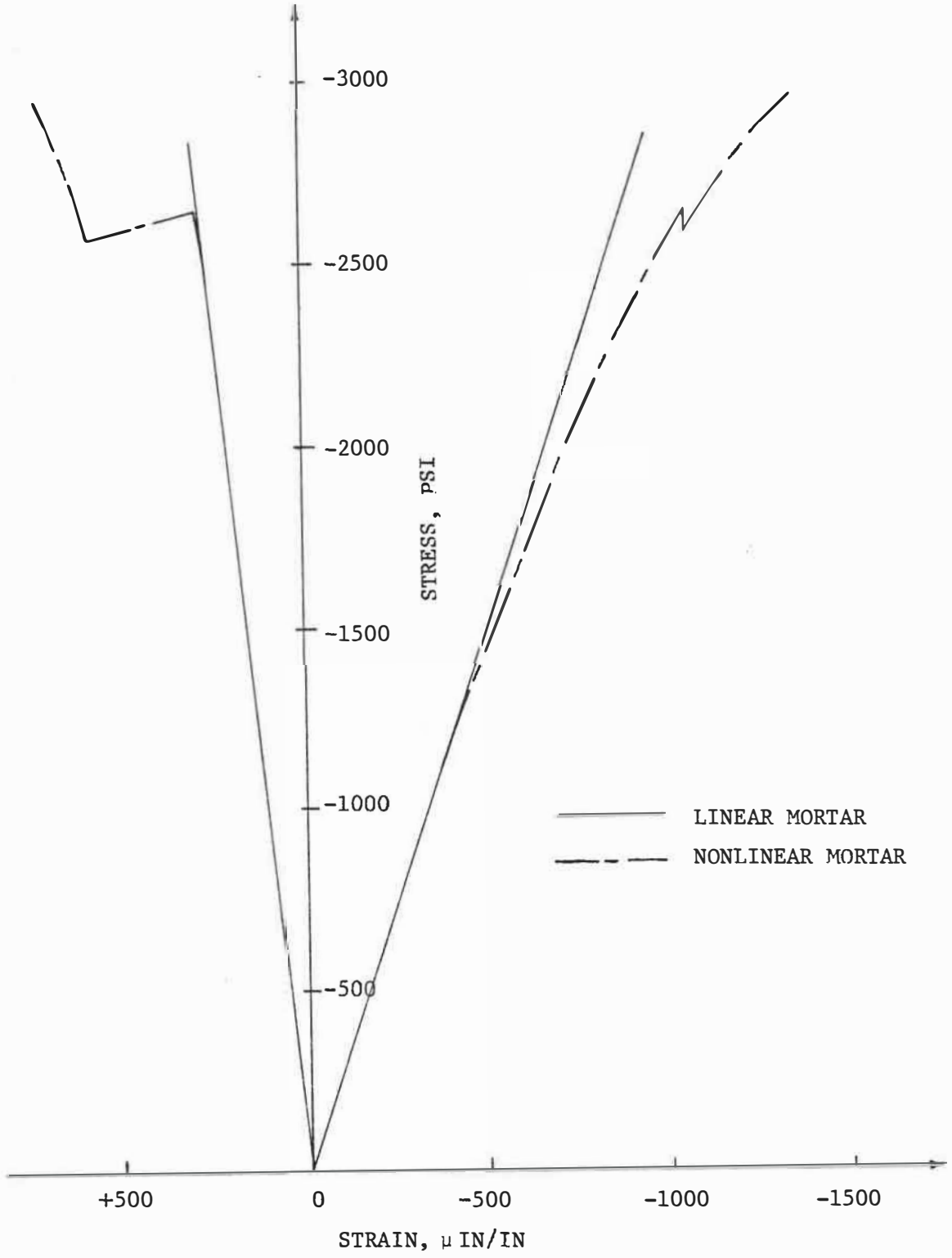

FIGURE 4.6. STRESS-STRAIN CURVE FOR CONCRETE WITH ZERO TENSILE AND COHESIVE STRENGTH OF INTERFACE

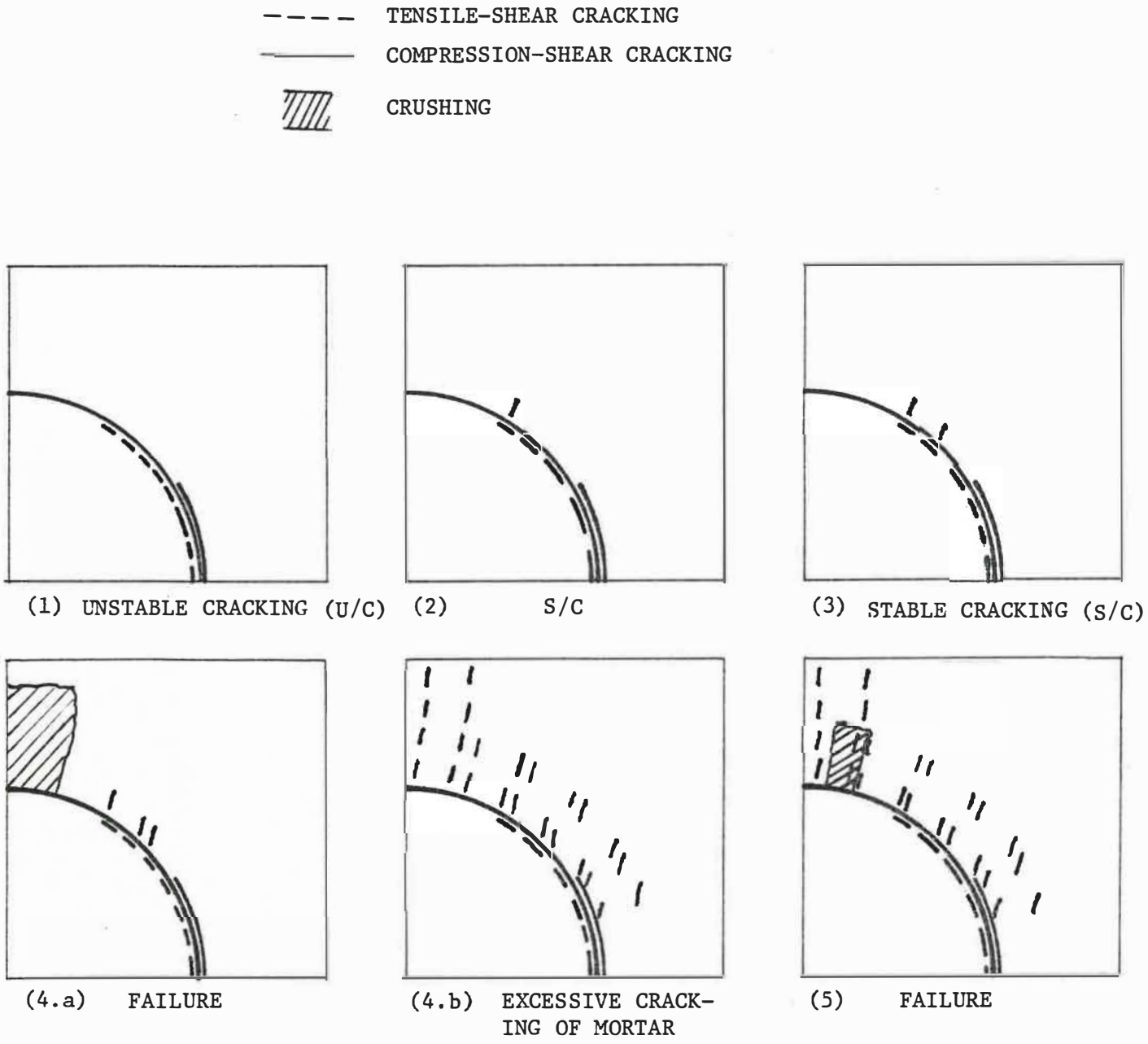

FIGURE 4.7. CRACKING MAPS FOR CONCRETE WITH ZERO TENSILE AND COHESIVE INTERFACIAL STRENGTH (STRAINS AND STRESSES AT DIFFERENT "STAGES" OF CRACKING ARE SHOWN IN TABLE 4.2.)

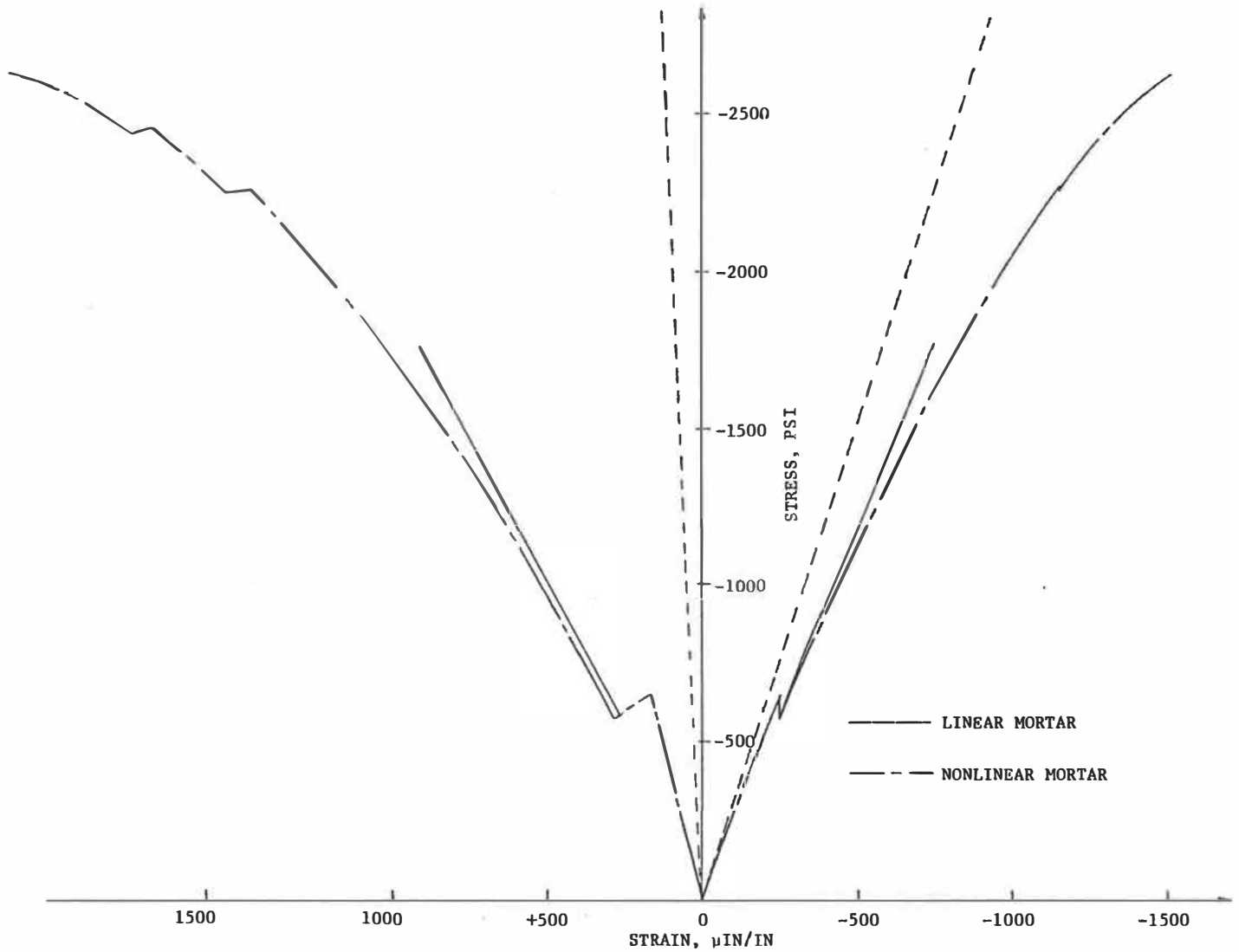

FIGURE 4.8. STRESS-STRAIN CURVES FOR CONCRETE WITH ZERO INTERFACIAL STRENGTH

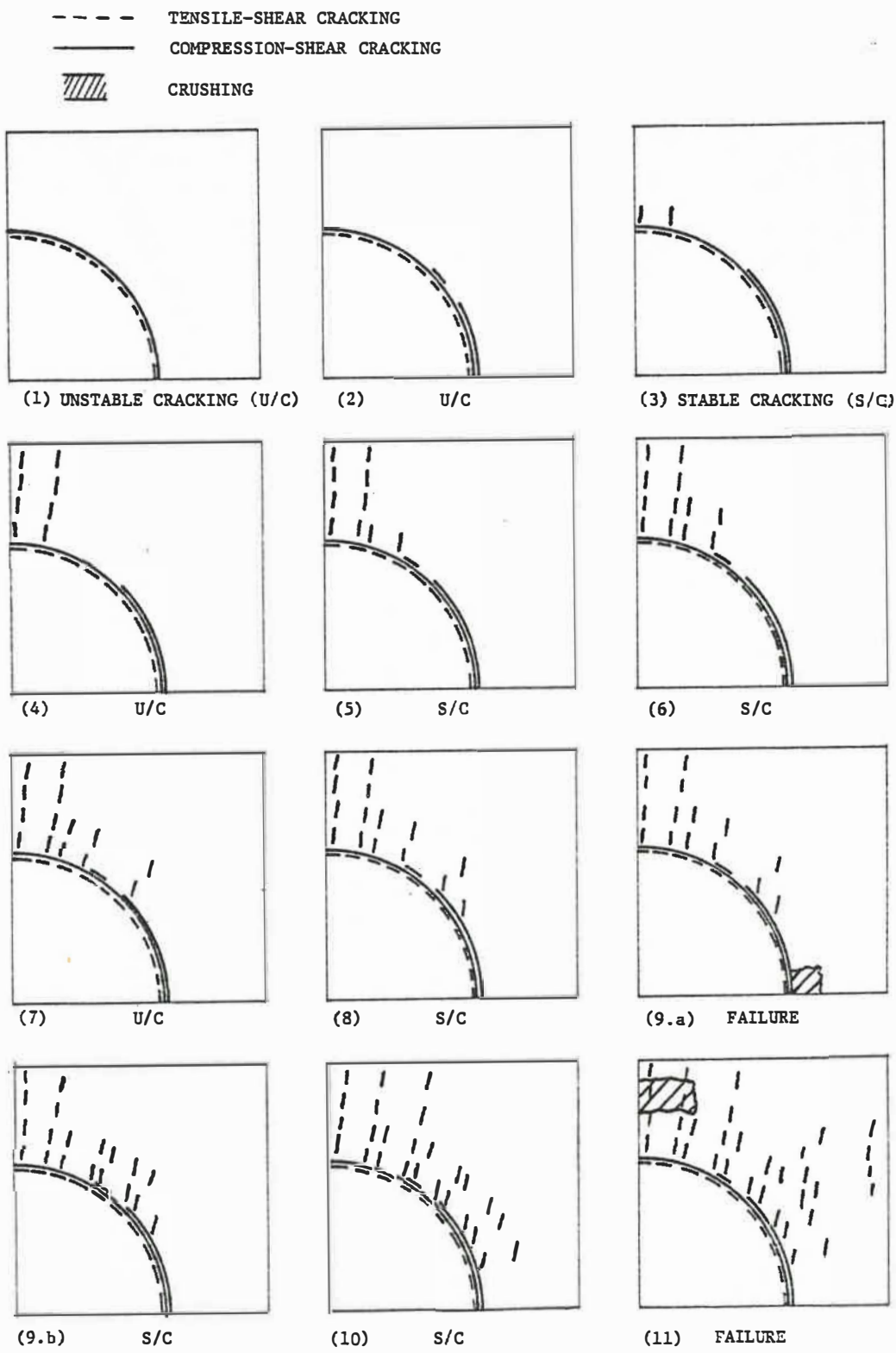

FIGURE 4.9. CRACKING MAPS FOR CONCRETE WITH ZERO INTERFACIAL STRENGTH (STRESSES AND STRAINS AT DIFFERENT "STAGES" OF CRACKING ARE SHOWN IN TABLE 4.3.)

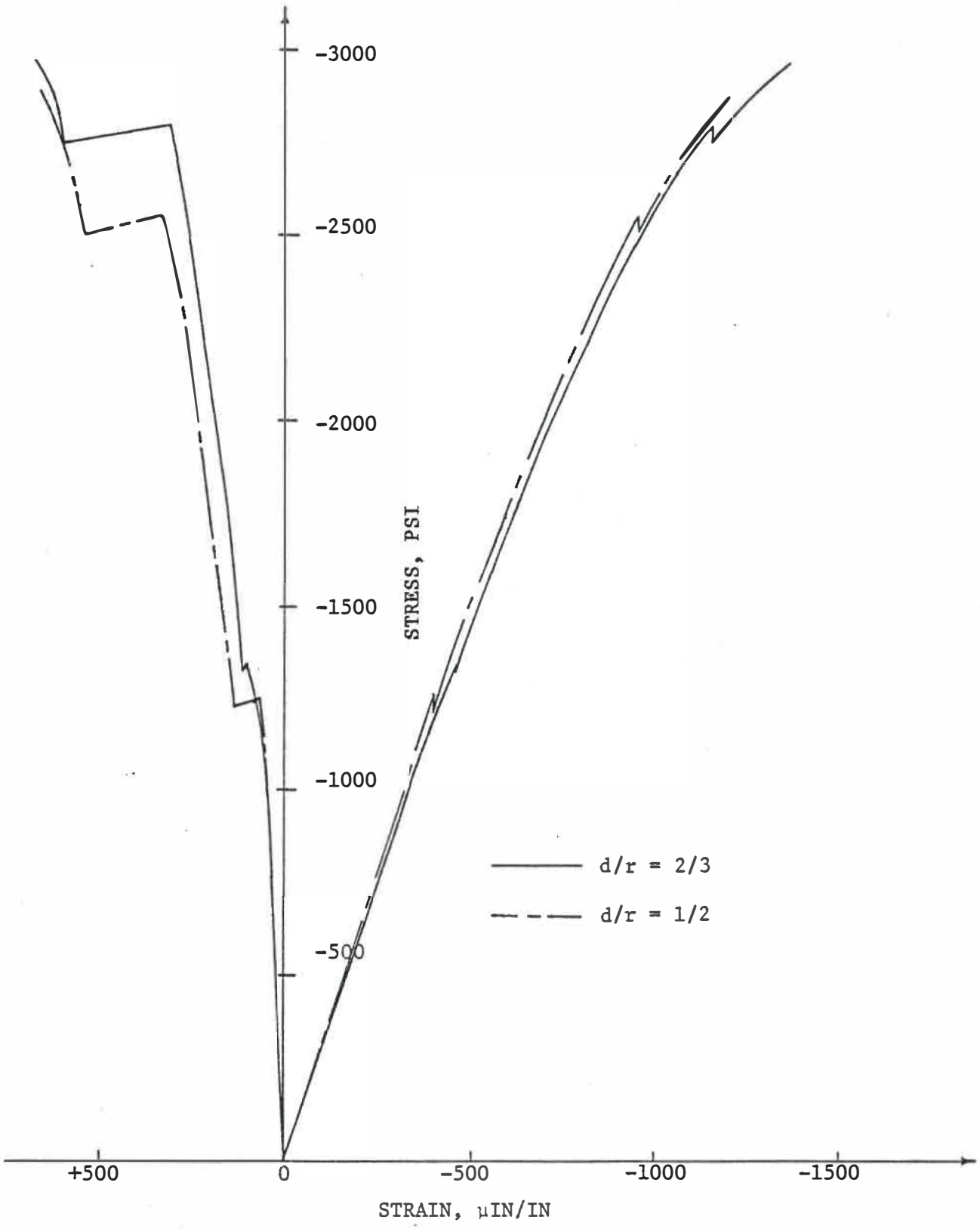

FIGURE 4.10. ANALYTICAL STRESS-STRAIN CURVES FOR CONCRETE WITH NORMAL INTERFACIAL STRENGTH AND NONLINEAR MORTAR

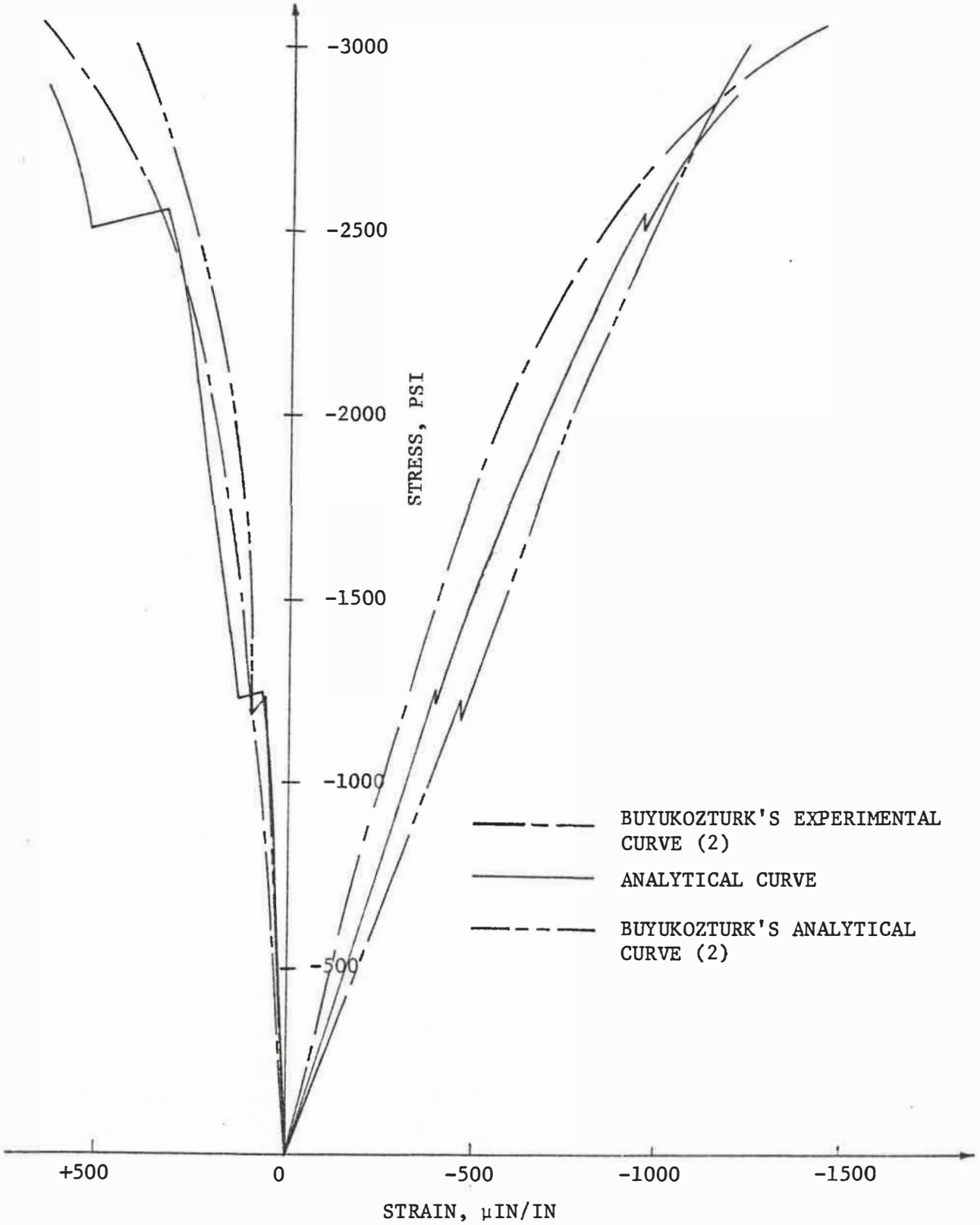

FIGURE 4.11. COMPARISON OF EXPERIMENTAL AND ANALYTICAL STRESS-STRAIN CURVES

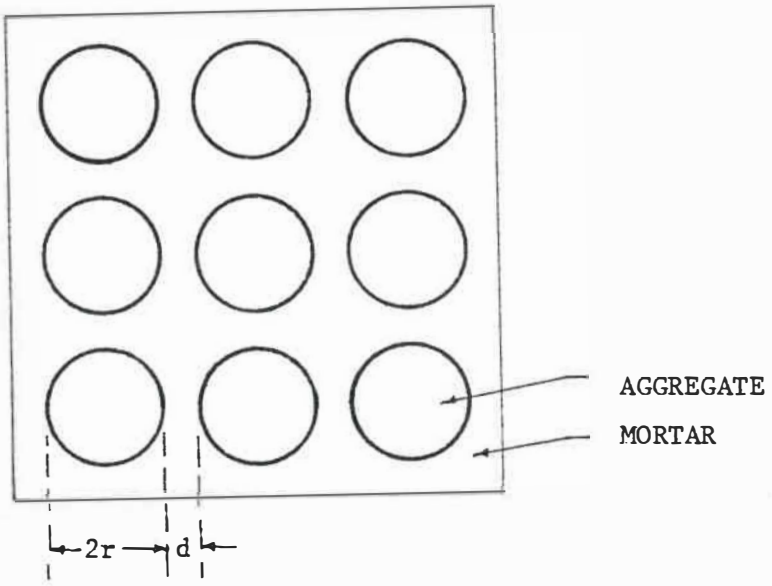

FIGURE 4.12. BUYUKOZTURK'S MODEL OF CONCRETE (2)

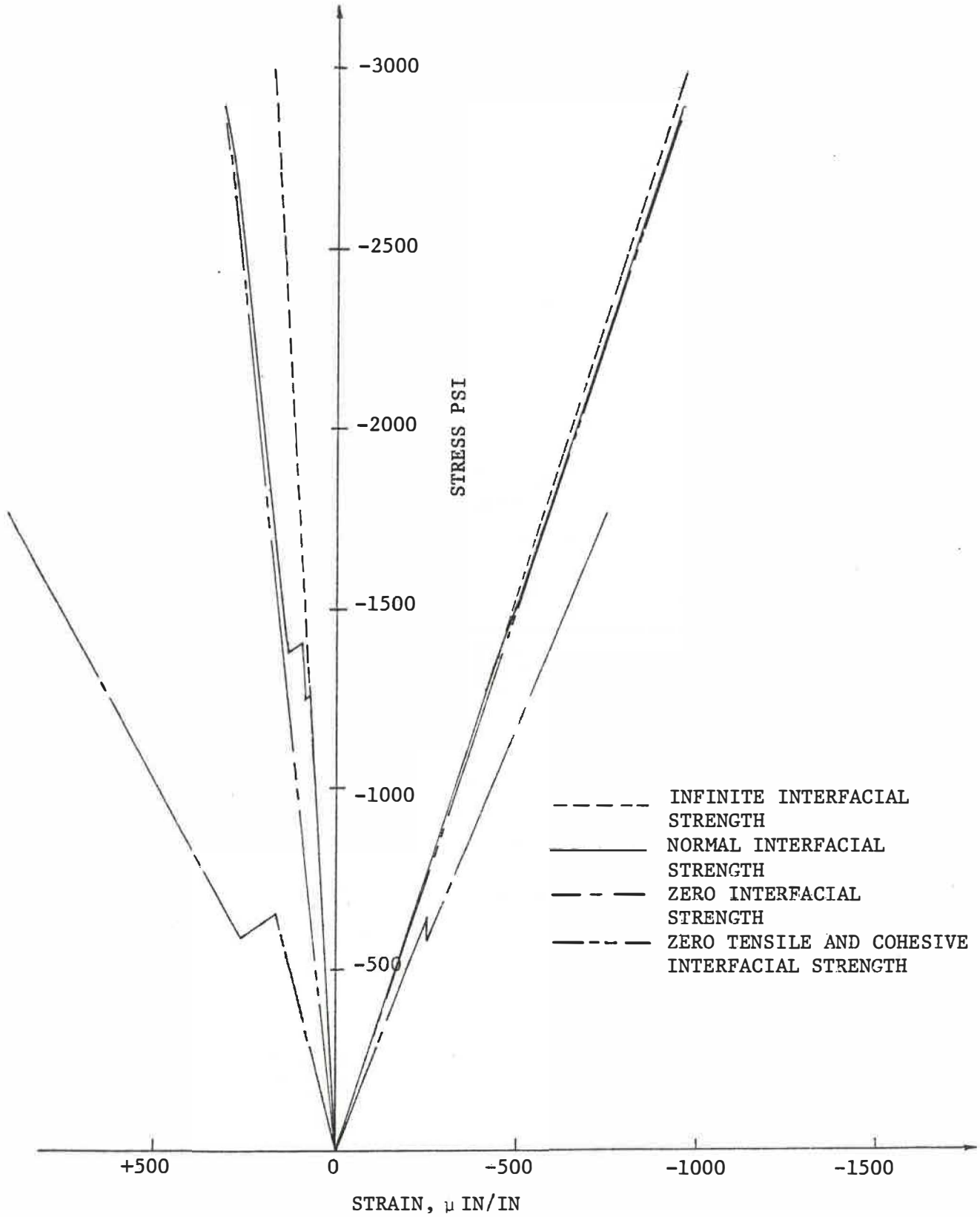

FIGURE 4.13. STRESS-STRAIN CURVES FOR CONCRETE WITH LINEAR REPRESENTATION OF MORTAR

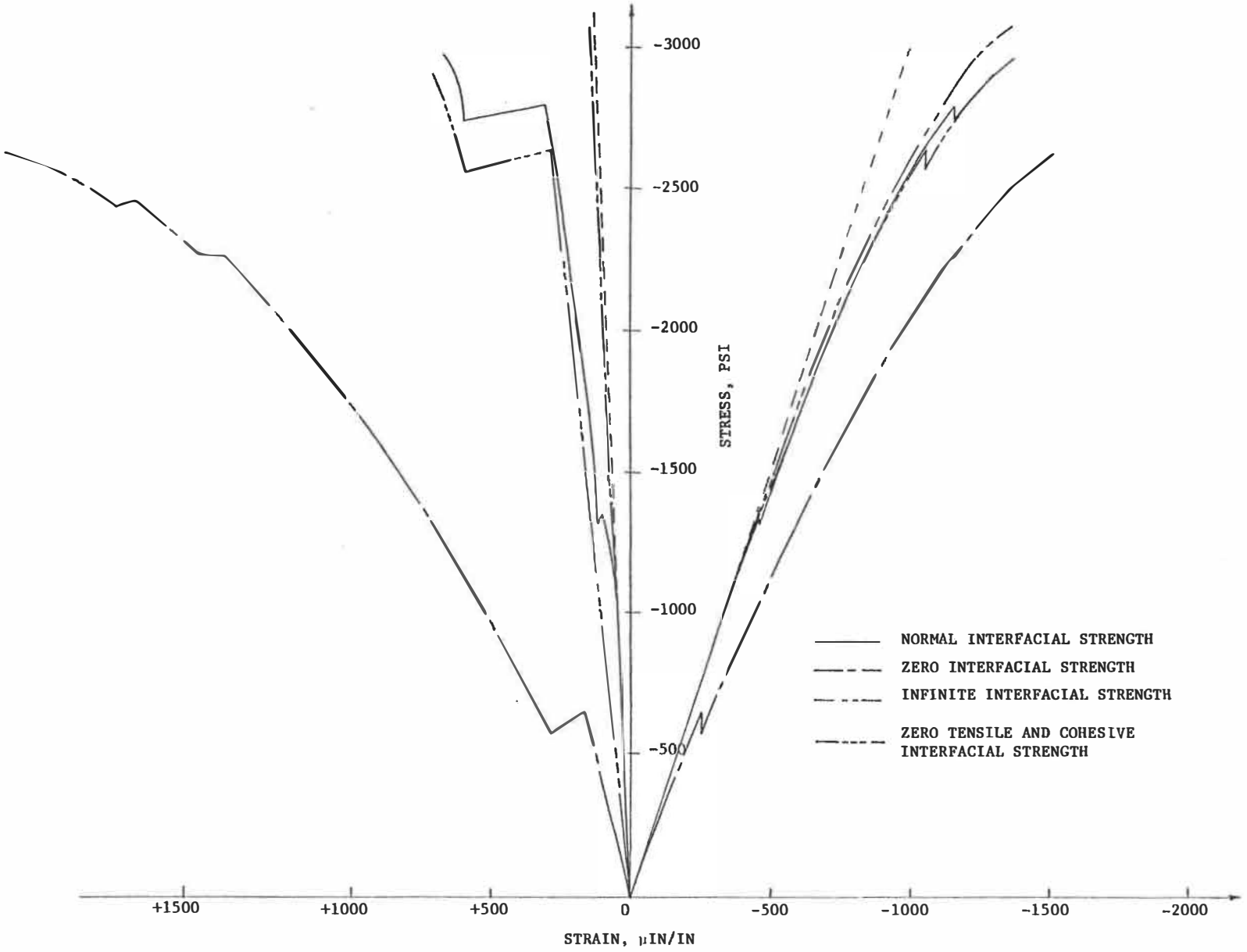

FIGURE 4.14. STRESS-STRAIN CURVES FOR CONCRETE WITH NONLINEAR MORTAR

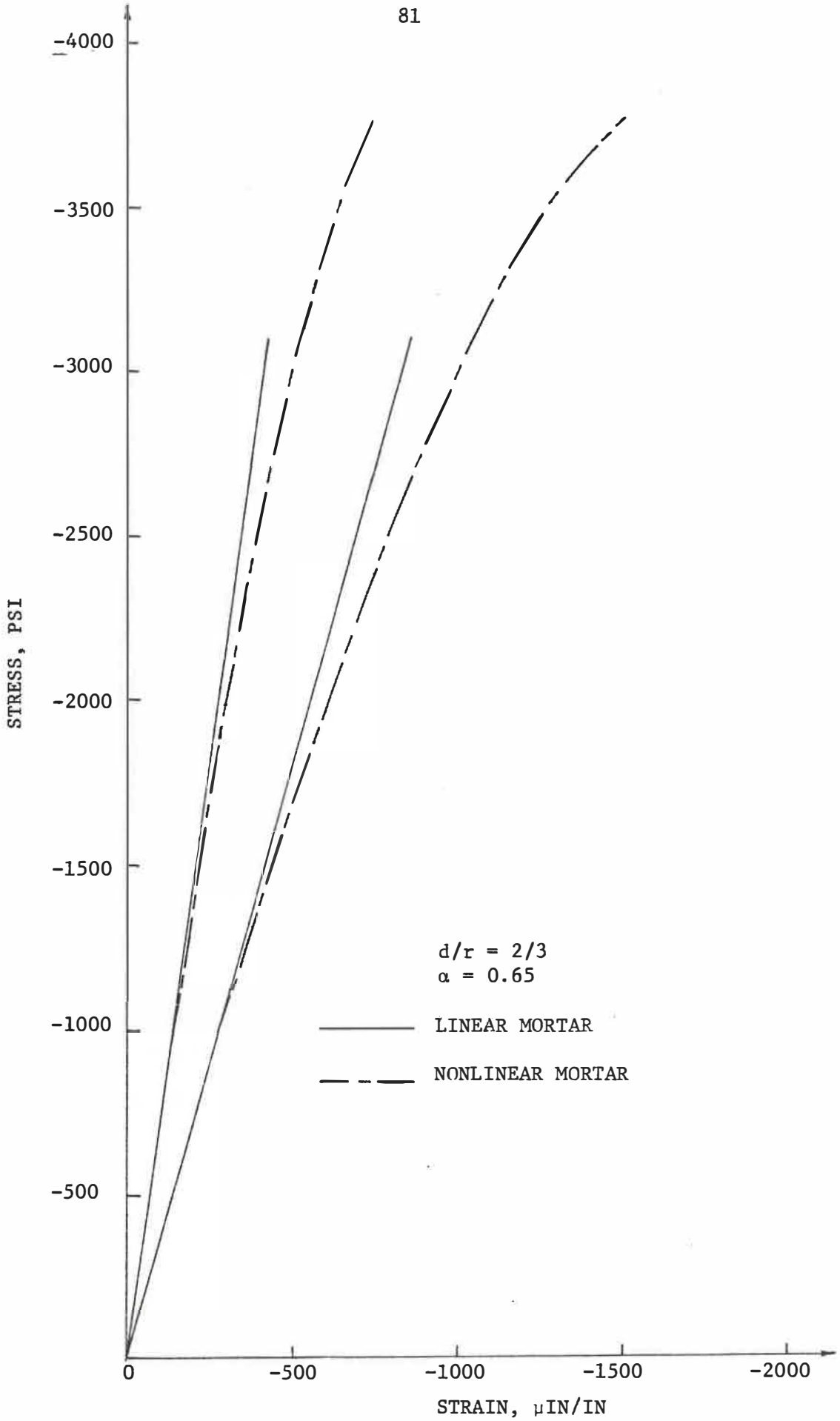

FIGURE 4.15. ANALYTICAL BIAXIAL STRESS-STRAIN CURVES

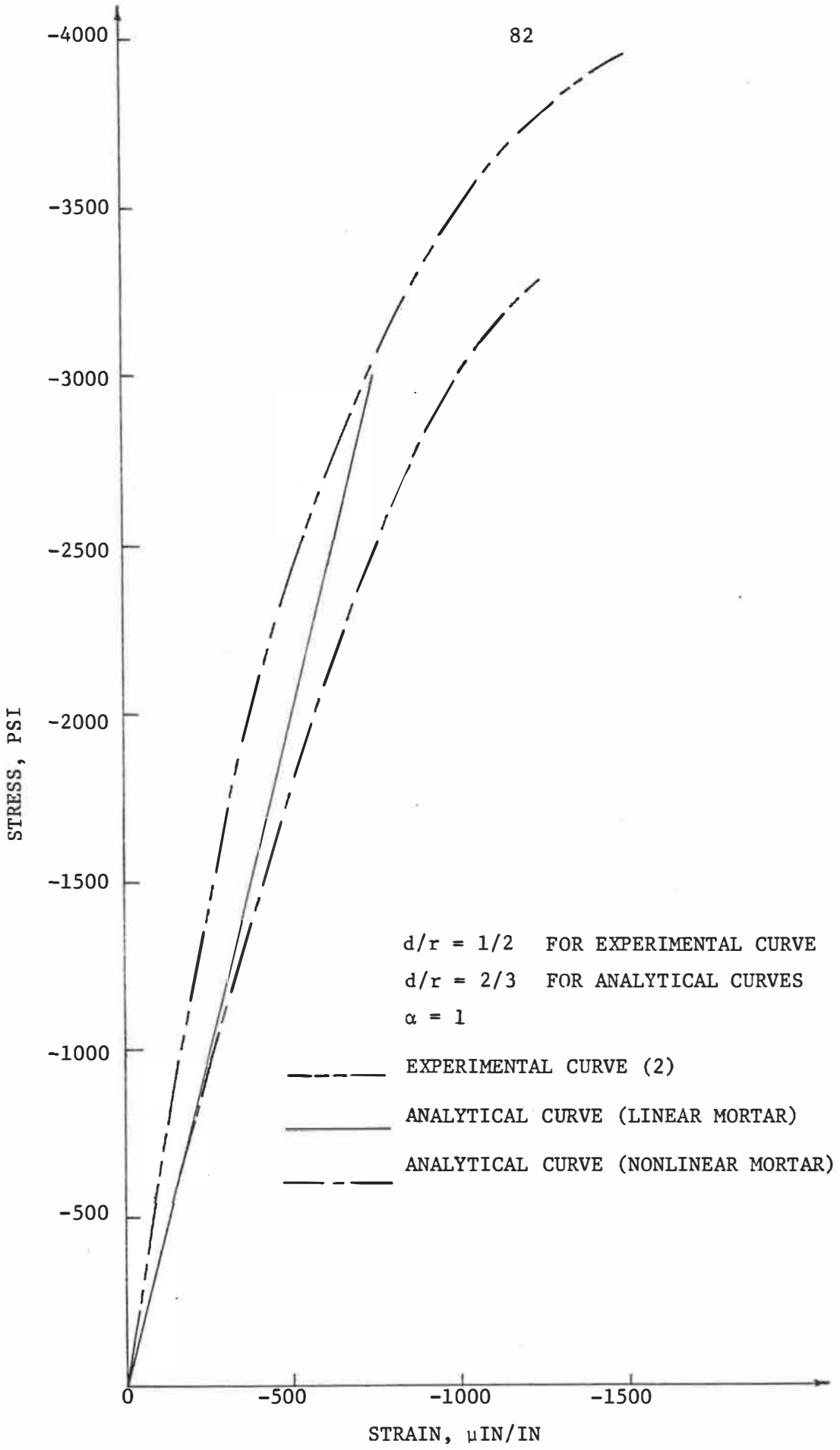

FIGURE 4.16. COMPARISON OF EXPERIMENTAL AND ANALYTICAL BIAXIAL STRESS-STRAIN CURVES FOR CONCRETE.

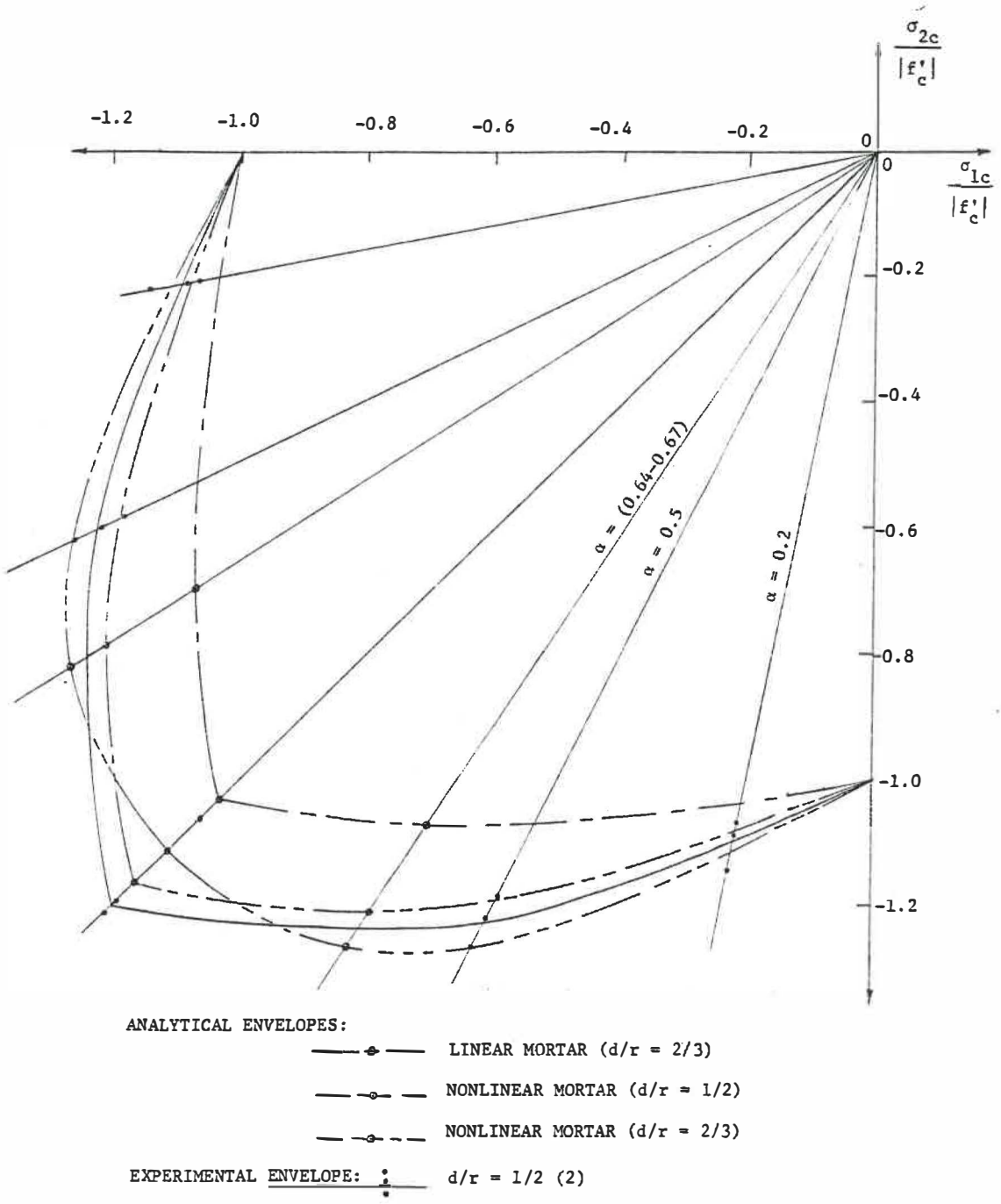

FIGURE 4.17. BIAXIAL STRENGTH ENVELOPES

CRINC LABORATORIES

Chemical Engineering Low Temperature Laboratory

Remote Sensing Laboratory

Flight Research Laboratory

Chemical Engineering Heat Transfer Laboratory

Nuclear Engineering Laboratory

Environmental Health Engineering Laboratory

Information Processing Laboratory

Water Resources Institute

Technical Transfer Laboratory

Air Pollution Laboratory

Satellite Applications Laboratory

CRINC